Author Manuscript

Author Manuscript

Author Manuscript

Author Manuscript

HHS Public Access

Author manuscript

Cell Rep. Author manuscript; available in PMC 2024 April 10.

Published in final edited form as:

Cell Rep. 2024 March 26; 43(3): 113815. doi:10.1016/j.celrep.2024.113815.

Deficiency of lncRNA *MERRICAL* abrogates macrophage chemotaxis and diabetes-associated atherosclerosis

Jingshu Chen[1,6], **Anurag Jamaiyar**[1,6], **Winona Wu**[1,6], **Yi Hu**[1], **Rulin Zhuang**[1,2], **Grasiele Sausen**[1], **Henry S. Cheng**[1], **Camila de Oliveira Vaz**[1], **Daniel Pérez-Cremades**[1,3], **Aspasia Tzani**[1], **Michael G. McCoy**[1], **Carmel Assa**[1], **Samuel Eley**[1], **Vinay Randhawa**[1], **Kwangwoon Lee**[4], **Jorge Plutzky**[1], **Naomi M. Hamburg**[5], **Marc S. Sabatine**[1], **Mark W. Feinberg**[1,7,*]

[1]Cardiovascular Division, Department of Medicine, Brigham and Women's Hospital, Harvard Medical School, Boston, MA 02115, USA

[2]Department of Cardiovascular Surgery, Shanghai East Hospital, Tongji University School of Medicine, Shanghai 200120, China

[3]Department of Physiology, University of Valencia and INCLIVA Biomedical Research Institute, 46010 Valencia, Spain

[4]Division of Genetics, Department of Medicine, Brigham and Women's Hospital, Harvard Medical School, Boston, MA 02115, USA

[5]Evans Department of Medicine and Whitaker Cardiovascular Institute, Boston University School of Medicine, Boston, MA 02118, USA

[6]These authors contributed equally

[7]Lead contact

SUMMARY

Diabetes-associated atherosclerosis involves excessive immune cell recruitment and plaque formation. However, the mechanisms remain poorly understood. Transcriptomic analysis of the aortic intima in *Ldlr*$^{-/-}$ mice on a high-fat, high-sucrose-containing (HFSC) diet identifies a macrophage-enriched nuclear long noncoding RNA (lncRNA), *MERRICAL* (macrophage-enriched lncRNA regulates inflammation, chemotaxis, and atherosclerosis). *MERRICAL* expression increases by 249% in intimal lesions during progression. lncRNA-mRNA pair genomic mapping reveals that *MERRICAL* positively correlates with the chemokines Ccl3 and Ccl4. MERRICAL-deficient macrophages exhibit lower Ccl3 and Ccl4 expression, chemotaxis, and

This is an open access article under the CC BY-NC-ND license (http://creativecommons.org/licenses/by-nc-nd/4.0/).

*Correspondence: mfeinberg@bwh.harvard.edu.

AUTHOR CONTRIBUTIONS

M.W.F. and J.C. conceived the hypothesis. J.C., A.J., Y.H., W.W., H.S.C., C.V., R.Z., G.S., J.C., and A.T. performed the experiments. J.C., Y.H., R.Z., A.J., D.P.-C., W.W., M.G.M., C.A., S.E., V.R., J.P., K.L., N.M.H., M.S.S., and M.W.F. designed or interpreted the results. J.C., A.J., and W.W. provided critical reagents. J.C. and M.W.F. wrote the manuscript.

SUPPLEMENTAL INFORMATION

Supplemental information can be found online at https://doi.org/10.1016/j.celrep.2024.113815.

DECLARATION OF INTERESTS

The authors declare no competing interests.

Author Manuscript Author Manuscript Author Manuscript Author Manuscript

inflammatory responses. Mechanistically, *MERRICAL* guides the WDR5-MLL1 complex to activate CCL3 and CCL4 transcription via H3K4me3 modification. *MERRICAL* deficiency in HFSC diet-fed *Ldlr*$^{-/-}$ mice reduces lesion formation by 74% in the aortic sinus and 86% in the descending aorta by inhibiting leukocyte recruitment into the aortic wall and pro-inflammatory responses. These findings unveil a regulatory mechanism whereby a macrophage-enriched lncRNA potently inhibits chemotactic responses, alleviating lesion progression in diabetes.

Graphical abstract

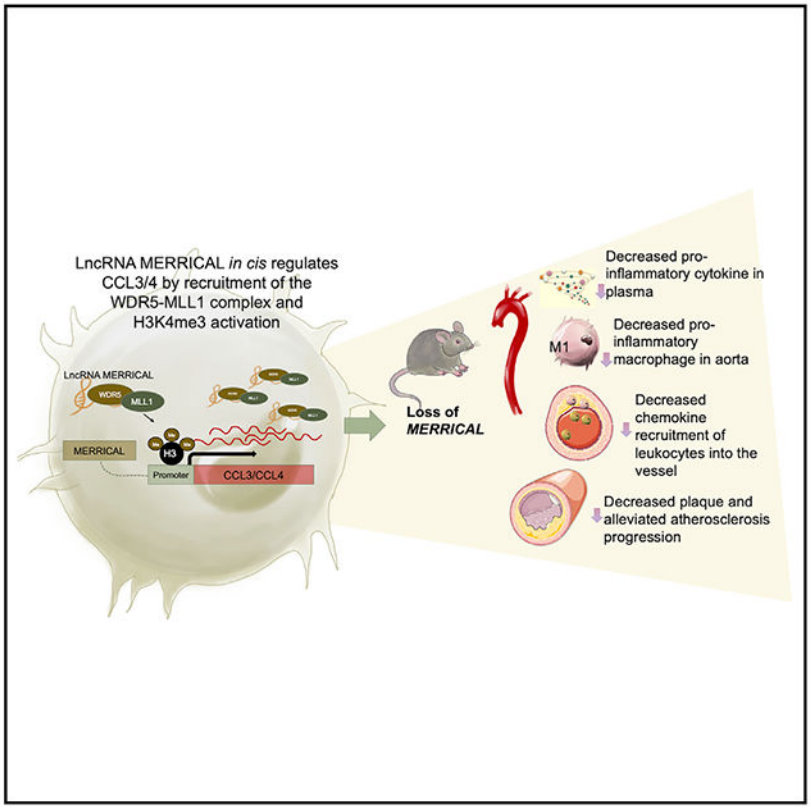

In brief

Diabetes-associated atherosclerosis involves excessive immune cell recruitment and plaque formation that is more resistant to standard therapy. Chen et al. discovered a macrophage-enriched long noncoding RNA named *MERRICAL* in diabetes-associated atherosclerosis. *MERRICAL* regulated chemotaxis and inflammatory responses, and systemic deficiency of *MERRICAL* markedly reduced lesion formation in a diabetes-associated atherosclerosis mouse model.

INTRODUCTION

The increased prevalence of diabetes mellitus in recent years has triggered a global health crisis, particularly by contributing to accelerated atherosclerosis and associated cardiovascular morbidity and mortality.[1] Type 2 diabetes mellitus, a complex and multifactorial metabolic disease, is characterized by the cardinal features of hyperglycemia,

Author Manuscript Author Manuscript Author Manuscript Author Manuscript

hyperinsulinemia, dyslipidemia, and chronic inflammation.[2] Prolonged exposure to these metabolic alterations is now recognized as a major factor in the pathogenesis of atherosclerosis in diabetes.[3] Accumulating studies highlight that chronic inflammation coupled with dysregulation of macrophage effector functions may be a critical link between lesion progression and diabetes.[4] Following recruitment and differentiation of circulating monocytes into the vessel wall, lesional macrophages phagocytose modified low-density lipoprotein particles and contribute to the growth and subsequent de-stabilization of plaques through secretion of pro-inflammatory mediators, such as chemokines and cytokines.[4–7] However, significant gaps remain in the molecular underpinnings that regulate macrophage chemokine/cytokine secretion and the pro-inflammatory response in diabetes-associated atherosclerosis.

Advances in genome-wide transcriptome analysis demonstrated that only 2% of the mammalian genome is transcribed into protein-coding RNAs (mRNAs),[8,9] indicating that the majority of the mammalian genome is utilized for generating transcripts that lack protein-coding potential. These transcripts are defined as noncoding RNAs (ncRNAs).[10–12] Currently, ncRNAs are broadly classified into two major groups based on size: (1) a variable class of small ncRNAs (<200 bp) and (2) transcripts that exceed 200 bp and are broadly defined as long ncRNA (lncRNA).[13,14] An accumulating body of evidence indicates that lncRNAs play crucial roles in regulating key cellular processes and are dysregulated in diverse disease states, including atherosclerosis.[15–24]

Surprisingly, lncRNAs discovered to date in cardiovascular disease function through a variety of mechanisms, ranging from interactions between RNA, chromatin, DNA, and protein to cell signaling.[10] While some lncRNAs have been reported to act in *trans* and pervasively regulate gene expression from a different genomic location, a growing proportion of lncRNAs have been reported to act in *cis* and function as local effectors to regulate the expression of neighboring mRNA transcripts.[25–27] For example, several co-expressed neighboring mRNA-lncRNA pairs have been identified in endothelial cells with positive correlations in vascular disease models.[19,28,29] However, whether such *cis*-acting lncRNAs participate in the inflammatory and chemotactic response in macrophages in the development of diabetes-associated atherosclerosis remains to be investigated.

There are several established diabetic atherosclerosis mouse models, including a streptozotocin (STZ)-induced type 1 diabetes model[30–32] and a genetic diet-induced type 2 diabetic mouse model.[33] In this study, we utilized a diet-induced diabetic atherosclerosis mouse model by placing *Ldlr*$^{-/-}$ mice on a high-fat, high-sucrose-containing (HFSC) diet in a similar manner as described previously.[34] *Ldlr*$^{-/-}$ mice on this HFSC diet exhibited hyperglycemia, glucose and insulin resistance, and hyperlipidemia and developed atherosclerosis with accelerated lesion formation.[34] We performed a transcriptomics analysis on the aortic intima during lesion progression from *Ldlr*$^{-/-}$ mice under HFSC diet conditions and identified neighboring mRNA-lncRNA pairs differentially expressed with atherosclerosis progression. One lncRNA that was captured in this analysis showed a strong positive correlation with a well-studied group of chemokine genes in the *Ccl* family. We characterized and performed functional experiments with this lncRNA, which we termed macrophage-enriched lncRNA regulates inflammation, chemotaxis, and atherosclerosis

Author Manuscript Author Manuscript Author Manuscript Author Manuscript

(*MERRICAL*) due to its critical role in macrophage chemotaxis and inflammation during the development of diabetes-associated atherosclerosis in $Ldlr^{-/-}$ mice. Overall, these findings provide insights into the pathobiology of a broad range of chronic disease states associated with the maladaptive macrophage chemotactic response in diabetes.

RESULTS

Discovery of *MERRICAL*, a coordinately regulated lncRNA with a group of chemokine genes in diabetes-associated atherosclerosis

We aimed to identify significantly regulated lncRNA candidates in the aortic intima during the progression phase of diabetes-associated atherosclerosis. We applied a diet-induced diabetic atherosclerosis mouse model by placing $Ldlr^{-/-}$ mice on an HFSC diet. After 12 weeks of HFSC diet feeding, $Ldlr^{-/-}$ mice exhibited hyperglycemia, glucose and insulin intolerance, and hyperlipidemia, as reported previously.[34]

Transcriptomic analysis was performed on RNA samples derived from the aortic intima of $Ldlr^{-/-}$ mice after a progression phase of 0, 2, and 12 weeks on the HFSC diet (groups 1–3) (Figure 1A). RNA sequencing (RNA-seq) profiling captured a total of 16,917 mRNAs and 2,807 lncRNAs (Figure 1B). DEseq2 analysis was performed to identify significantly differentially expressed transcripts. In total, 140 lncRNAs and 2,763 mRNAs were differentially expressed (false discovery rate [FDR] < 0.05) at the 12-week progression time point (G3). We chose to focus our subsequent analysis on the 12-week progression time point, as phenotypic changes at this time point were more magnified in the development of diabetic atherosclerosis.[34] The top dysregulated noncoding transcript was the lncRNA AI662270 (hereafter called *MERRICAL*), which is upregulated at 12 weeks of lesion progression (Figures 1C and 1D).

Given the potential for lncRNAs to regulate their neighboring genes,[35] we aimed to discover “local” regulatory lncRNAs involved in the progression of atherosclerosis. Compared with the physical distance of lncRNA and mRNA pairs, chromatin organization appears to play a more important role, as mRNA-lncRNA pairs localized within the same or adjacent topologically associating domain (TAD) showed the highest correlation, irrespective of the distance between them.[28] We performed an analysis of differentially expressed (DE)-mRNA DE-lncRNA pairs and matched the pairs back to a genomic Hi-C database[36] and found that there were 75 mRNA-lncRNA pairs within 500-kb distance (Figures 1E, S1A, and S1B). Surprisingly, among those pairs, the lncRNA *MERRICAL* positively correlated with several mRNA transcripts in close proximity (Figures 1E, 1F, S1B, and S1C) that comprised a family of chemokine genes known to be closely associated with chemotaxis and pro-inflammatory responses in the progression of atherosclerosis.[37] Interestingly, we found that only the chemokine genes exhibited upregulated expression during the progression phase, whereas the Schlafen (SLFN) genes did not show any such change (Figure 1F). Because of its expression pattern and function, as explored below, we named this lncRNA *MERRICAL*.

Author Manuscript Author Manuscript Author Manuscript Author Manuscript

Identification of the lncRNA *MERRICAL* in the intima of atherosclerotic lesions

The lncRNA *MERRICAL* is a total of four spliced variants (Figure S1C). We performed statistical analysis of differential transcript usage for *MERRICAL* and found that the transcript ENSMUST00000216842.2 (1,428 bp) is the dominant isoform and was significantly upregulated in the progression (G3) group (Figures S1D and S1E).

Studies have shown that lncRNAs are enriched in a tissue- or cell-specific manner that can exert profound phenotypic effects.[38,39] The lncRNA *MERRICAL* was enriched in the aortic intima compared with the media isolated from $Ldlr^{-/-}$ mice on the HFSC diet (Figure 2A). Tissue profiling revealed that the lncRNA *MERRICAL* was highly enriched in the bone marrow (BM), spleen, thymus, and peripheral blood mononuclear cells (PBMCs) compared with the liver and lungs (Figure 2B). The aortic intima was not only enriched in endothelial cells but also highly expressed several leukocyte markers in atherosclerotic mice.[40] Using magnetic bead-isolated aortic cells ($CD45^+$ leukocytes, $CD31^+$ endothelial cells, $CD90.2^+$ fibroblasts, and $aSMA^+$ smooth muscle cells), we found that lncRNA *MERRICAL* expression was uniquely enriched in $CD45^+$ leukocytes (Figure 2C). Consistent enrichment of the lncRNA *MERRICAL* was also observed in the uniform manifold approximation and projection (UMAP) of single-cell RNA-seq from mouse aortic cells (Figures 2F and S13). Among the macrophage and monocyte cluster, 81.8% of *MERRICAL*'s expression is expressed in this cluster (Figure 2L). Moreover, by comparing different types of immune cells, the lncRNA *MERRICAL* had the highest expression in macrophages, especially activated peritoneal macrophages (Figure 2D). The expression of the lncRNA *MERRICAL* was exponentially upregulated with the differentiation of BM-derived macrophages (BMDMs) and in pro-inflammatory M1-like macrophages (Figure 2E).

MERRICAL is annotated as an lncRNA in both the Ensembl database and NCBI. We validated this transcript's coding potential by first checking the coding probability using the *in silico* coding potential assessment tool (CPAT) and found that *MERRICAL* had a score similar to those of other well-described lncRNAs, such as MALAT1[41,42] or CARMN[20,43] (Figure 2G). Consequently, to further validate any peptide coding potential, the *MERRICAL* sequence was cloned upstream of the p3 × FLAG-CMV plasmid, transfected into HEK293T cells, and immunoblotted for a FLAG tag. No peptide or protein from *MERRICAL* overexpression was detected (Figure 2H). RNA *in situ* hybridization (RNA-ISH) demonstrated that *MERRICAL* localized to the nucleus of BMDMs (Figure 2I), which was further validated by quantitative real-time polymerase chain reaction (PCR) of nuclear and cytoplasmic fractions (Figure 2J).To further assess the cellular specificity in atherosclerotic lesions, RNA-ISH identified that *MERRICAL* (nuclear staining, green) was found in close proximity to the cytoplasmic macrophage marker F4/80 (antibody stained in pink) in atherosclerotic lesions, indicating high specificity for lesional macrophages (Figure 2K).

MERRICAL-deficient macrophages inhibit pro-inflammatory responses and chemokine CCL3/CCL4 expression *in vitro*

To explore the role of the lncRNA *MERRICAL* in regulating macrophage functions, we performed a transcriptomics analysis in *MERRICAL* knockdown (KD) BMDMs in a resting

Author Manuscript Author Manuscript Author Manuscript Author Manuscript

phase (control) and a pro-inflammatory phase (LPS [lipopolysaccharide]) (Figures S2C and S2D). *MERRICAL* gapmeR-mediated KD effectively reduced *MERRICAL* expression in both control and LPS-treated BMDMs (Figures S2A, S2B, and 4B). RNA-seq (GSE235419) captured 222 DE genes (DEGs) in the M0 control BMDMs and 5,827 DEGs in the M1 LPS-treated BMDMs (FDR < 0.05) (Figures 3A and S3C–S3E). Ingenuity Pathway Analysis (IPA) of canonical pathways in combination with R package GOplot[44] were used on the set of DEGs (adjusted $p < 0.05$). Notably, several inflammatory pathways were shown in the top dysregulated pathways; i.e., "inflammasome pathway," "IL-2 signaling," "IL-3 signaling," "STAT3 pathway," "chemokine signaling," and "IL-8 signaling" (Figures 3B and 3C). GOchord plots of the top DEGs associated with these enriched pathways revealed several downregulated pro-inflammatory transcripts, including *Ccl3* and *Ccl4*, the two neighboring genes of *MERRICAL* (Figures 3C and 3D). Interestingly, we found that 173 significantly regulated genes in common between the decreased DEGs from BMDM RNA-seq (*MERRICAL* KD vs. non-specific [NS] control) and the upregulated DEGs in the athero-intimal RNA-seq (progression G3 vs. control G1) (Figure 3E). IPA canonical pathway analysis of these overlapping 173 genes revealed that the top enriched pathways included "inflammatory response" and "chemotaxis." *Ccl3* and *Ccl4* were identified as the top decreased DEGs in the *MERRICAL* KD BMDMs, and as the top upregulated DEGs during the progression of diabetic atherosclerosis (G3 versus G1) (Figure 3F). Together, these results indicate that the lncRNA *MERRICAL* contributes to the regulation of inflammatory response and chemotaxis, potentially through in *cis* regulation of its neighboring genes *Ccl3* and *Ccl4*.

Loss and gain of function of the lncRNA *MERRICAL* regulate chemotaxis and pro-inflammatory response *in vitro*

The results from the RNA-seq suggested that *MERRICAL* plays a critical role in regulating immune responses in BMDMs under pro-inflammatory stimuli. To further investigate this possibility, we next conducted loss and gain-of-function studies by both knocking down *MERRICAL* using gapmeR (loss of function) and overexpressing *MERRICAL* using an expression vector carrying the full-length sequence of *MERRICAL* (gain of function). Both quantitative real-time PCR and RNA-ISH confirmed the efficiency of KD (80%) of *MERRICAL* in BMDMs (Figures 4A, 4B, and S2B). Cell viability and apoptosis were not affected after *MERRICAL* KD in BMDMs (Figures S3A–S3E). Expression of *Ccl3* and *Ccl4* was decreased at both the gene and protein levels, as shown by quantitative real-time PCR and mouse cytokine multiplex assays (Figures 4C–4E), while other chemokine neighbor genes of the lncRNA *MERRICAL* were not affected (Figures S4A and S4B). We also treated the BMDMs with palmitic acid, a saturated fatty acid that is known to promote inflammation and insulin resistance.[45,46] *MERRICAL* expression was potently induced in response to palmitic acid in BMDMs (Figure S6A). Consistently, *MERRICAL* KD in BMDMs reduced the expression of *Ccl3* and *Ccl4* in the presence of palmitic acid treatment, as shown by quantitative real-time PCR (Figures S6B and S6C). However, *MERRICAL* KD was found not to affect oxidized low-density lipoprotein (oxLDL) uptake (Figure S6D) or phagocytosis (Figure S6E).

Author Manuscript Author Manuscript Author Manuscript Author Manuscript

MERRICAL KD BMDMs also exhibited a strong reduction in the adhesion of calcein-labeled mouse PBMCs to endothelial cell (bEnd3 cells) monolayers in the presence of supernatants from *MERRICAL* KD or control BMDMs (Figures 4F and S4C). Consistent with this finding, there was a significant decrease in BMDM migration using supernatants of the *MERRICAL* KD BMDMs in the Transwell migration assay (Figures S4D and S4E). To further investigate whether the migration difference in *MERRICAL* KD was associated with CCL3 and CCL4, we performed Transwell migration assays with neutralization antibodies to CCL3 and CCL4 (Figure 4G). We observed significantly decreased migration in the NS control group treated with neutralization antibodies to CCL3 and CCL4 compared with the immunoglobulin G (IgG) control. The decrease with these neutralization antibodies was markedly blunted in the *MERRICAL* KD group, highlighting the dependent nature of this migratory effect on CCL3 and CCL4.

Consistent results were further shown by profiling the cytokine antibody arrays of 42 cytokines related to immunity and inflammation from the culture supernatants of BMDMs (KD vs. NS control) (Figure S4E). In contrast, gain of function by overexpression of the lncRNA *MERRICAL* in BMDMs (Figures S5A–S5C) upregulated *Ccl3* and *Ccl4* expression but not other chemokines or cytokines in the presence or absence of pro-inflammatory stimuli by quantitative real-time PCR (Figures 4H, 4I, S5D, and S5E). These loss- and gain-of function results in BMDMs highlight that the lncRNA *MERRICAL* likely plays an important role in chemotaxis by regulating its neighboring chemokine genes *Ccl3* and *Ccl4*.

The lncRNA *MERRICAL* regulates CCL3 and CCL4 transcription through interaction with H3K4me3

Since the lncRNA *MERRICAL* exhibited predominant nuclear localization (Figures 2I and 2J), we next explored the possibility that the lncRNA *MERRICAL* controls *Ccl3* and *Ccl4* gene expression by regulating their transcription. *MERRICAL* expression was upregulated in a time-dependent manner in response to LPS. *Ccl3* and *Ccl4* expression was measured in *MERRICAL* KD and overexpressing BMDMs after stimulation with LPS. *Ccl3* and *Ccl4* mRNA expression was significantly reduced in KD BMDMs in a time-dependent manner (Figures 5A–5D). We performed chromatin immunoprecipitation (ChIP) followed by qPCR to monitor the recruitment of RNA polymerase II (RNA Pol II) to regulatory regions of *Ccl3* and *Ccl4* that were down-regulated with *MERRICAL* deficiency. RNA Pol II recruitment to the transcription start site (TSS) of *Ccl3* and *Ccl4* was observed in the LPS-stimulated BMDMs; however, these responses were ameliorated in the *MERRICAL* KD BMDMs (Figures S7D and S7E). Consistent with these observations, the inducible recruitment of RNA Pol II at *Ccl3* and *Ccl4* TSS sites was further enhanced in the *MERRICAL* overexpression BMDMs (Figures S7F and S7G). These observations strongly suggest that the lncRNA *MERRICAL* regulates the expression of *Ccl3* and *Ccl4* at the level of transcription.

Several studies have suggested lncRNAs exert their activity in cooperation with chromatin-modifying enzymes to promote epigenetic activation.[47] Specifically, lncRNAs can bind to chromatin remodeling complexes, including polycomb repressive complexes, and other

Author Manuscript Author Manuscript Author Manuscript Author Manuscript

epigenetic modifiers to modulate downstream gene expression and serve as scaffolds for the histone modification complex.[47,48]

Several chemokine gene promoters are enriched for H3 methylation dynamics. One well-known transcription-permissive marker is H3K4me3 (trimethylation of histone H3 at lycine 4).[49–51] Some lncRNAs interact with chromatin-remodeling complexes and catalyze H3K4me3 in the promoter region of the targeted genes.[47,52,53] Based on this possibility, we hypothesized that lncRNA *MERRICAL* may interact with chromatin-modifying enzymes and, in turn, epigenetically regulate *Ccl3* and *Ccl4* expression. We performed lncRNA pulldown assays and found that H3K4me3, a known transcription activation marker, showed specifically stronger binding to *MERRICAL* in LPS-stimulated BMDMs compared with the LacZ control (Figure 5E). In contrast, there was no difference in H3K4me2 or H3K9me2 (histone H3 lysine 9 dimethylation) indicating specificity for H3K4me3. RNA immunoprecipitation (IP) studies showed consistent binding efficiency between H3K4me3 and *MERRICAL* (Figures 5F and S7H).

We next performed the cleavage under targets and release using nuclease (CUT&RUN) assay[54] to explore chromatin-associated interaction between H3K4me3 and DNA loci under various conditions, including *MERRICAL* KD and NS groups treated with PBS (control) or LPS (2 h). Our findings revealed that LPS treatment increased the presence of H3K4me3 in the genomic areas of CCL3 and CCL4. Conversely, in the *MERRICAL* KD LPS group, we observed a reduction in H3K4me3 enrichment specifically within the genomic regions of CCL3 and CCL4 compared with the NS LPS group. Intriguingly, this diminished H3K4me3 enrichment was exclusive to the genome regions of CCL3 and CCL4, unlike neighboring genes, such as Wfdc17, Wfdc18, and CCL5, and other chemokine genes, such as CCL12 (Figure 5G). In addition, we performed ChIP-qPCR to quantify H3K4me3 near the TSS of *Ccl3* and *Ccl4*, which were transcriptionally regulated by *MERRICAL*. H3K4me3 levels on the TSS of *Ccl3* and *Ccl4* were decreased in LPS-stimulated *MERRICAL*-deficient BMDMs (Figures 5G and 5H). In contrast, H3K4me3 enrichment on the TSS of *Ccl3* and *Ccl4* was upregulated in BMDMs overexpressed with *MERRICAL* (Figures 5J and 5K).

Based on our data demonstrating the regulatory role of *MERRICAL* in the H3K4me3 modification on the promoter region of *Ccl3* and *Ccl4*, we hypothesized that *MERRICAL* interacts physically with *Ccl3* and *Ccl4* at their respective promoter regions. To investigate this, we employed a chromatin isolation by RNA purification (ChIRP) assay which displayed specific enrichment for *MERRICAL* at the promoter regions of *Ccl3* and *Ccl4* (Figures 5L and 5M). Conversely, no significant enrichment was observed at the classic pro-inflammatory gene interleukin-1β (IL-1β) promoter (Figure S7I).

H3K4 methylation is mediated by several SET (Su(var)3–9, enhancer of zeste, trithorax) domain-containing methyltransferases, including mixed-lineage leukemia 1–5 (MLL1-MLL5) and SET1A/B.[55] We utilized the RNA-seq data to trace whether any of these were inversely regulated in response to LPS in the NS control group compared with the *MERRICAL* KD group in the presence of LPS. Among all comparisons, we found that MLL1 (KMT2A) was the top upregulated family member in LPS-treated vs. control in BMDMs and was also markedly downregulated in the LPS-treated *MERRICAL* KD group

Author Manuscript Author Manuscript Author Manuscript Author Manuscript

compared with LPS-treated NS controls (Figure 6A). MLL1 in particular exerts its activity through interactions with a complex that includes WDR5. Mechanistically, at the gene promoter level, MLL1 engages with the subunit WDR5, an RNA-binding adapter protein that recognizes H3K4 methylation. This interaction typically leads to the activation of targeted genes. To investigate the functional importance of the MLL1-WDR5 complex in gene regulation, we treated BMDMs with MM102, a small-molecule inhibitor specifically designed to block the interaction between WDR5 and MLL1.[56] As a result, we observed a significant reduction in the transcription of the *Ccl3* and *Ccl4* genes (Figures 6B and 6C). This finding highlights the critical role of the MLL1-WDR5 complex in the activation of H3K4me3 at the promoters of the CCL3 and CCL4 genes, emphasizing the necessity of this complex for gene activation.

To investigate the potential role of the lncRNA *MERRICAL* in conjunction with WDR5, we performed IP experiments targeting MLL1 and WDR5. These experiments were carried out under both NS control conditions and *MERRICAL* KD conditions in BMDMs stimulated with LPS. Remarkably, LPS treatment for 4 h resulted in an upregulated interaction between WDR5 and MLL1, while the deficiency of *MERRICAL* completely abolished this interaction (Figure 6D).

To further explore the potential binding between *MERRICAL* and WDR5, we employed the RNA-protein interaction prediction method.[57] This analysis indicated a predicted binding affinity of the nucleotides spanning 950–1,100 of *MERRICAL* to WDR5 (Figure S8A). Subsequently, we experimentally tested the direct binding of the lncRNA *MERRICAL* to WDR5 using RNA IP. The results demonstrated markedly higher binding efficiency between the lncRNA *MERRICAL* and WDR5 compared with the IgG control, an effect enhanced in the presence of LPS (Figure 6E). In contrast, there was no *MERRICAL* binding to other reported atherosclerosis-associated lncRNAs, including CARMN[20] or SNHG12[15] (Figure S8B). Taken together, our findings suggest that the lncRNA *MERRICAL* binds with WDR5, facilitating the WDR5-MLL1 interactions and promoting the H3K4me3 epigenetic modification at the promoter region of the CCL3 and CCL4 genes (Figure 6F).

MERRICAL silencing inhibits pro-inflammatory responses and diabetes-associated atherosclerosis

To explore the role of the lncRNA *MERRICAL* in regulating the progression of diabetes-associated atherosclerosis, $Ldlr^{-/-}$ mice on the HFSC diet were injected retro-orbitally (r.o.) with NS control or *MERRICAL* gapmeRs over 12 weeks (Figure 7A). After 12 weeks on the HFSC diet, gapmeR-mediated silencing of the lncRNA *MERRICAL* reduced its expression in the aortic intima by 80% (Figure 7B). The silencing effect was also observed in PBMCs, the spleen, and BM but not in the lungs or liver (Figures S9A–S9E). Mouse weight gain (Figure S10A), glucose and insulin tolerance (Figures S10B and S10C), and lipid metabolism, including cholesterol, triglyceride, and high-density lipoprotein (HDL) levels, were not affected by lncRNA *MERRICAL* KD (Figures S10D–S10F). Analysis of atherosclerotic lesion formation revealed a 74% decrease in lesion area by oil red O (ORO) staining (Figure 7E) and an 86% decrease in lesion area of the arch and descending aorta by light sheet fluorescent microscopy[58] (Figures 7F; Videos S1 and S2) after *MERRICAL*

Author Manuscript Author Manuscript Author Manuscript Author Manuscript

KD in mice. As shown by immunohistochemistry, *MERRICAL*-deficient lesions at the aortic sinus showed significantly decreased accumulation $CD68^+$ macrophages by 76% as quantified by flow cytometry and by 88% as quantified by immunofluorescent staining, with no changes in $aSMA^+$ (anti-alpha smooth muscle actin) smooth muscle cells (SMCs) after normalization to the lesion area (Figure 7G). In addition to $CD68^+$ macrophages, we also observed significantly decreased accumulation of $CD4^+$ T cells by 87.5% and a non-significant trend in $CD8^+$ T cells in the aortic root in *MERRICAL* KD mice compared with the control (Figure S12). Further quantification of leukocyte subsets in the aorta by flow cytometry analysis showed that the percentages of $CD45^+$ leukocytes, $F4/80^+$ macrophages, and $CD86^+$ M1-like macrophages were significantly decreased in the *MERRICAL* KD mice, whereas the percentage of $CD206^+$ M2-like macrophages was significantly upregulated in the *MERRICAL* KD group (Figures 7H and S11). There was no effect of MERRICAL KD on the BM cell $CD45^+$ leukocyte, $CD115^+$ monocyte, or Ly6C monocytic populations (Figure S11D). Based on the *in vitro* regulation of *MERRICAL* on chemokine and inflammatory markers, we performed quantitative real-time PCR and found that *Ccl3/4* and *Il1-β* were significantly inhibited in the *MERRICAL* KD aortic intima (Figures 7C, 7D, and S9F). We further profiled the circulating cytokines in the plasma using mouse cytokine multiplex assays, and, interestingly, *Ccl3* and *Ccl4* were the top significantly decreased cytokines in plasma from the *MERRICAL* KD group (Figures 7I and 7J). Collectively, these data strongly support the theory that *MERRICAL*-deficient mice on an HFSC diet have decreased *Ccl3* and *Ccl4* expression, reduced chemokine recruitment of leukocytes into the blood vessel wall, and markedly alleviated progression of diabetes-associated atherosclerosis.

DISCUSSION

In this study, we applied a diet-induced diabetic atherosclerosis mouse model by placing *Ldlr*−/− mice on an HFSC diet. After 12 weeks HFSC diet, *Ldlr*−/− mice exhibited hyperglycemia, glucose and insulin intolerance, and hyperlipidemia (Figures S14A–S14L). Changes in cholesterol levels were assessed during the progression and regression phases, showing that the HFSC diet was a more aggressive diet and had a delayed regression phenotype (Figures S14D–S14L) compared with the conventional high-cholesterol diet. We aimed to identify significantly regulated lncRNA candidates in the aortic intima during the progression or regression phases of diabetes-associated atherosclerosis.

To date, projects such as ENCODE (the Encyclopedia of DNA Elements), LNCipedia, and the HUGO Gene Nomenclature Committee have distinguished lncRNAs based on expression levels and functions in processing of RNA, DNA, or protein.[59] However, there are still numerous unidentified lncRNAs with unknown functions in regulating gene expression and signaling pathways in metabolic diseases such as diabetes-associated atherosclerosis. Our study aimed to identify functional lncRNA candidates that are involved in the robust chronic inflammation and accelerated lipid deposition manifest in the development of diabetes-associated atherosclerosis.

Among the identified lncRNAs pervasively transcribed in the mammalian genome, some lncRNAs have been shown to recruit regulatory complexes through RNA-protein

Author Manuscript Author Manuscript Author Manuscript Author Manuscript

interactions to influence the expression of nearby genes.[47,58,60–63] Thus, we sought to screen significantly correlated lncRNA-mRNA pairs using intima RNA-seq data from the HFSC diet-induced atherosclerosis mouse model. Based on recent Hi-C genomic sequencing studies, the genome is compartmentalized into chromatin neighborhoods that have been referred to as TADs[64] that highlight that genomic distance alone does not explain the actual physical interactions between transcripts and that lncRNA-mRNA pairs can be dictated by these higher-order chromatin neighborhoods or TADs. We mapped our lncRNA-mRNA pairs to the Hi-C genomic database and defined a total of 75 lncRNA-mRNA pairs. Among these pairs, one of the lncRNAs that positively correlated with a group of chemokine genes implicated in inflammation and chemotaxis during the progression of atherosclerosis attracted our attention. Based on cell and tissue profiling and the *in vitro/in vivo* functional assays, we named this lncRNA *MERRICAL*. *MERRICAL* was the top-expressing lncRNA from differential expression analysis over 12 weeks of atherosclerotic progression on the HFSC diet, and the expression of the lncRNA *MERRICAL* significantly decreased in the regression phase (24-week time point, Figure S14M). Other lncRNAs may certainly play a contributory role in this process and will be of interest for future study.

Several lines of evidence support a pro-inflammatory role of the lncRNA *MERRICAL* in macrophages. Based on the transcriptomic analysis of *MERRICAL*-deficient BMDMs in both M0 (resting phase) and M1 (pro-inflammatory phase), surprisingly, we found about 5,800 DEGs in the M1 phase comparison but only 222 DEGs in the M0 phase comparison. This huge spike of DEGs between *MERRICAL* KD and the NS control indicated that the lncRNA *MERRICAL* may play a causal role in regulating the pro-inflammatory response. The observed *MERRICAL* KD effect might also be more prominently displayed in the highly activated M1 state, further amplifying the differences in gene expression. Pathway enrichment of the DEGs identified from the M1 BMDM comparison showed a variety of inflammation-associated pathways, including chemotaxis and innate immune response. Among the DEGs, *Ccl3* and *Ccl4*, which were earlier captured as neighboring transcripts of *MERRICAL*, were the top significantly decreased genes in *MERRICAL* KD BMDMs. *In vitro* loss and gain of function of *MERRICAL* consistently indicated that the lncRNA *MERRICAL* positively regulated its neighboring genes *Ccl3* and *Ccl4* in *cis* both under inflammatory stimuli such as LPS or diabetes-associated stimuli such as palmitic acid. While the chemotaxis signaling pathway was among the top enriched pathways in response to *MERRICAL* KD, it will be of interest for future studies to explore whether other pathways may harbor potential direct targets regulated by *MERRICAL*.

Uncovering the mechanistic modes of actions of lncRNAs remains a laborious task due to multiplexed interactions between proteins, DNA, and lncRNAs.[65] The localization of lncRNAs can be closely related to its function in cells.[66] While the majority of lncRNAs are found to be nucleus enriched, the amount present in the cytoplasmic fraction is often variable. In the case of the lncRNA *MERRICAL*, using RNA-ISH and cellular fractions, we found that the lncRNA *MERRICAL* was predominantly localized in the nucleus of BMDMs. Nucleus-enriched lncRNAs are often found to interact with transcription factors and histone modifiers.[66] Consistent with its nuclear localization, we found that the lncRNA *MERRICAL* controls expression of *Ccl3* and *Ccl4* at the transcriptional level. Because of the rapid nature of regulation of *Ccl3* and *Ccl4* by *MERRICAL* in gain-

Author Manuscript Author Manuscript Author Manuscript Author Manuscript

or loss-of-function studies, we hypothesized that *MERRICAL* may epigenetically modify these chemokines. An RNA pull-down assay showed that lncRNA *MERRICAL* possessed a particularly strong interaction with a histone activation marker, H3K4me3, compared with other histone modifiers. Several chemokine gene promoters are enriched for H3K4 mono-, di-, and trimethylation.[49,50] After conducting a CUT&RUN assay,[54] we explored the chromatin-associated interactions between H3K4me3 and DNA loci in response to LPS and *MERRICAL* KD in macrophages. Under the proinflammatory stimulus of LPS, we identified heightened enrichment peaks on the genomic regions of CCL3 and CCL4 (Figure 5G). This suggests that LPS stimulation triggers increased H3K4me3 enrichment on the genomic elements of CCL3 and CCL4, subsequently activating their expression. In contrast, *MERRICAL* KD diminished this enrichment of H3K4me3 in the presence of LPS compared with the NS group, both in global genomic regulation and in the CCL3 and CCL4 genomic region (Figures S7B and S7C). Intriguingly, this diminished H3K4me3 enrichment was exclusive to the genome regions of CCL3 and CCL4, unlike neighboring genes, such as Wfdc17, Wfdc18, and CCL5, and other chemokine genes, such as CCL12 (Figure 5G). MLL1-WDR5 interaction has been found to be critical for facilitating H3K4me3 activation at the promoter region of targeted genes. Initially, we showed that treatment of macrophages with an MLL1-WDR5 interaction inhibitor resulted in decreased activation of *Ccl3* and *Ccl4*. This finding confirmed the dependency of chemokine activation, specifically *Ccl3* and *Ccl4*, on the H3K4me3 modification mediated by the interaction between MLL1 and WDR5. Furthermore, IP experiments between WDR5 and MLL1 revealed the complete loss of their interaction under lncRNA *MERRICAL* deficiency. Collectively, these findings support a mechanistic role of MERRICAL as a scaffold, regulating the activation of H3K4me3 on CCL3 and CCL4 by facilitating the interaction between the MLL1 and WDR5 complex. While the CUT&RUN assay demonstrates selectivity of the MERRICAL complex for the chemokines CCL3 and CCL4 in response to inflammatory stimuli in macrophages, future studies will be of interest to assess whether a specific motif may be involved in this process.

To further investigate the mechanism, we conducted RNA pull-down assays and observed a particularly strong interaction between the lncRNA *MERRICAL* and the histone activation marker H3K4me3 compared with other histone modifiers. These results collectively support a mechanism whereby the lncRNA *MERRICAL* binds to WDR5, facilitating the interaction between WDR5 and MLL1, orchestrating the deposition of H3K4me3 at the promoter region of *Ccl3* and *Ccl4*. Consequently, this leads to the activation of *Ccl3* and *Ccl4* transcription under inflammatory conditions. While WDR5-MLL1 is not a cell-specific complex, by virtue that *MERRICAL* is highly expressed in macrophages and strongly associates with WDR5-MLL1, this paradigm is likely to be primarily operative in macrophages and other immune cell types where *MERRICAL* is robustly expressed. Notably, we also observed a decrease in RNA Pol II enrichment at the TSS of *Ccl3* and *Ccl4* under *MERRICAL* KD conditions (Figures S7D and S7E) and increased in RNA Pol II enrichment under *MERRICAL* overexpression conditions (Figures S7F and S7G). Previous reports have indicated that loss of H3K4me3 results in a widespread decrease in transcriptional output, accompanied by RNA Pol II pausing and slower elongation.[67] Intriguingly, we found that there was a potential ortholog of *MERRICAL*, the

Author Manuscript Author Manuscript Author Manuscript Author Manuscript

lncRNA EPIC. This lncRNA showed remarkable conservation with *MERRICAL*, sharing 22 completely conserved sequences and overall 46% similarity. Moreover, our analysis using an RNA-protein interaction tool[68] predicted a strong interaction between the lncRNA EPIC and human WDR5, further highlighting its potential functional relevance in the context of WDR5-mediated processes. Further investigations are required to elucidate the role of *MERRICAL*-H3K4me3 in regulating RNA Pol II transcription pause-release and elongation specifically for the chemokine genes *Ccl3* and *Ccl4*. Additionally, exploring the function of the potential human ortholog of *MERRICAL*, the lncRNA EPIC1, will be informative for understanding macrophage-regulated immune responses in human disease.

Besides its genomic local function on *Ccl3* and *Ccl4*, we observed that numerous innate immune response signaling pathways were also regulated. These *in vivo* studies also showed that *MERRICAL*-deficient mice systemically inhibited inflammation with decreased shifting of pro-inflammatory Ly6chi monocytes in PBMCs (Figures S10C and S10D). It remains a possible mechanism that lncRNA *MERRICAL* may also act in *trans* to regulate other mRNAs via interaction with the RNA binding proteins WDR5-MLL1 and modified histones such as H3K4me3, and future studies will be needed to clarify this possibility. In addition to *MERRICAL* contributing to other transcriptional activation, the upstream transcriptional mechanisms controlling the lncRNA *MERRICAL* itself remains unclear. Our intimal RNA-seq and quantitative real-time PCR data showed that the lncRNA *MERRICAL* was induced in the intimal layer during atherosclerotic lesion progression (Figures 1C and 1D) and in response to inflammatory stimuli such as LPS or palmitic acid in BMDMs in a time-dependent manner (Figure S7A). Future investigation will be needed to help clarify the transcriptional regulation of *MERRICAL* since several studies have shown that the act of transcribing an lncRNA is sufficient to mediate chromatin remodeling.[69,70]

Our *in vivo* study showed that deficiency of the lncRNA *MERRICAL* inhibited leukocyte recruitment into the vessel wall and lesion formation, ultimately alleviating the development of diabetes-associated atherosclerosis. However, *MERRICAL* deficiency did not affect glucose metabolism or the circulating lipid profile in mice or BMDM cell oxLDL uptake or the phagocytosis process *in vitro*. These observations support the theory that the underlying molecular mechanisms of the lncRNA *MERRICAL* in regulating atherosclerosis is primarily through controlling macrophage chemotaxis and inflammatory responses. These studies build on the known roles of the chemokines Ccl3 and Ccl4 in promoting lesion progression in atherosclerosis models.[37,71] In addition, since the lncRNA *MERRICAL* is not only enriched in macrophages but also expressed in other immune cells, including T cells and B cells, future studies with a macrophage-specific *MERRICAL* knockout mouse model will be of interest to tease out the function of *MERRICAL* in macrophages compared with other cell subsets in atherosclerosis. The role of *MERRICAL* in other atherosclerosis paradigms, such as atherosclerotic regression in diabetes, or in lesion progression in the non-diabetic state will be of interest for future investigations.

In conclusion, we have identified the lncRNA *MERRICAL* as a macrophage-enriched lncRNA and a key regulator of chemotaxis and pro-inflammatory response in diabetes-associated atherosclerosis. The regulatory role of *MERRICAL* is in part through its in *cis* function by interacting with the WDR5-MLL1 complex to facilitate H3K4me3 and

Author Manuscript Author Manuscript Author Manuscript Author Manuscript

transcriptional activation at the *Ccl3* and *Ccl4* gene promoters. These findings establish mechanistic insights into macrophage-mediated chronic inflammation and chemotaxis in diabetic atherosclerosis and highlight targets for anti-inflammatory intervention.

Limitations of the study

While our study successfully demonstrated the impactful phenotype of atherosclerosis progression alleviation upon lncRNA *MERRICAL* KD using antisense oligonucleotides in $Ldlr^{-/-}$ mice fed an HFSC diet, it is important to note certain limitations. The use of antisense oligonucleotides did not enable precise targeting solely to aortic macrophages, thereby restricting our ability to discern the specific role of these cells or other cell types in this context. Future investigations should aim to explore the translational potential of this lncRNA within the human genome. Although we identified a potential ortholog, the lncRNA EPIC1, our primary focus was not directed toward this aspect.

STAR★METHODS

RESOURCE AVAILABILITY

Lead contact—Further information and requests for resources and reagents should be directed to and will be fulfilled by the Lead Contact, Mark Feinberg (mfeinberg@bwh.harvard.edu).

Materials availability—This study did not generate new unique reagents.

Data and code availability

- The NCBI GEO accession numbers is GSE235419 for the RNA-seq data
- This paper does not report original code.
- Any additional information required to reanalyze the data reported in this paper is available from the lead contact upon reasonable request.

EXPERIMENTAL MODEL AND STUDY PARTICIPANT DETAILS

Cell culture—bEnd.3 cells (ATCC, CRL-2299) were cultured in Dulbecco's Modified Eagle Medium/F12(1:1) (DMEM; Gibco, 11320-033) supplemented with 10% fetal bovine serum (FBS) and 1% Penicillin-streptomycin (P/S). HEK293T cells (ATCC, CRL-3216) were cultured in Dulbecco's Modified Eagle Medium (DMEM) supplemented with 10% FBS and 1% P/S. For culturing of bone marrow-derived macrophages (BMDMs), bone marrow was isolated from the femur and tibia of mice and cultured in Iscove's Modified Dulbecco's Medium (IMDM; Sigma, I3390) and 15% filtered L929 cell culture supernatant (containing monocyte-colony stimulating factor, M-CSF). The BMDMs were mature and ready for treatment after 7 days. For M1 activation, BMDMs were treated with 100 ng/mL LPS overnight; for M2 activation, BMDMs were treated with 10 ng/mL IL-4 overnight. Transfection was performed using Lipofectamine 2000 (Invitrogen) as described in the manufacturer's protocol. Customized GapmeRs for MERRICAL (Qiagen) or nonspecific control #1 (Qiagen) were used for transfection at 50 nM in BMDMs. Peritoneal macrophages (PM) were isolated according to method previously described.[4]

Author Manuscript Author Manuscript Author Manuscript Author Manuscript

Briefly, mice were intraperitoneally injected (i.p) with 1 mL 3.8% brewer's thioglycollate medium. After three days, treated mice were euthanized by CO2. 5 mL of cold PBS was injected into the peritoneal cavity, and peritoneal fluid was aspirated by needle syringe. Peritoneal fluid was centrifuged for 10 min (400 g, 4°C). The cell pellet was resuspended in RPMI medium and allowed to sit for 2 h and then the non-adherent cells were washed away with warm PBS.

Isolation of mouse peripheral blood mononuclear cells—Peripheral blood was collected by cardiac puncture of anesthetized mice, and 1:1 diluted with HBSS. PBMC were separated through density centrifugation (400 g at 20°C for 30 min) using histopaque-1077 gradient. The interphase fraction containing PBMCs was aspirated and red blood cells were lysed with ammonium chloride solution. After centrifugation (200 g, 5 min), pelleted PBMC was resuspended in RPMI medium supplemented with 10% FBS.

Animal experiments—Eight-week-old Ldlr−/− male mice were purchased from the Jackson Laboratory, and randomly divided into Control and *MERRICAL* knockdown group (n = 15 per group). All mice were continuously fed a high fat, high sucrose-containing diet (HFSC, Research Diets lnc., D09071704) for 12 weeks. Control group and *MERRICAL* knockdown mice were retro-orbitally (r.o.) injected with non-specific (NS) control or *MERRICAL* gapmeRs (20 mg/kg per mouse) once per week. C57BL/6J mice were purchased from Charles River. All animal experiments were approved by the Institutional Animal Care and Use Committee at Brigham and Women's Hospital and Harvard Medical School, Boston, MA and conducted in accordance with the National Institutes of Health Guide for the Care and Use of Laboratory Animals.

METHOD DETAILS

Intimal RNA isolation from aorta tissue—Isolation of medial and intimal RNA from aorta was conducted as previously described.[1,2] Briefly, mouse aorta between the heart and diaphragm was exposed, and then the peri-adventitial tissues were removed carefully. The cleaned aorta was carefully flushed with 1X PBS, and then flushed with 300 μL Trizol using 1 mL insulin needle. The intima eluate was collected into 1.5 mL Eppendorf tube and then intimal RNA was isolated as described above. The aorta leftover (media) was washed once with 1X PBS and the medial RNA was isolated by Trizol as described above.

Vector construction—Transcripts for *MERRICAL* (ENSMUST00000216842.2) were synthesized by Genewiz with 5′ KpnI and 3′NotI restriction sites. For overexpression, *MERRICAL* transcript was cloned into pcDNA3.1 using KpnI and NotI. For RNA synthesis *in vitro*, pcDNA3.1 containing MERRICAL transcript was sub-cloned into pBluescript SK II + using XbaI and Hind III. pcDNA3.1 vector containing MERRICAL transcript was sub-cloned upstream of p3xFLAG-CMV-14 expression vector (Sigma, E7908) using Hind III and Notl restriction site.

Protein-coding potential—In silico CPAT online algorithm was used for prediction of coding potential.[3] In total, 293T cells were transfected with 500 ng of either positive control (p3XFLAG-CMV-7-BAP) or p3xFLAG-CMV-14 expression vector containing *MERRICAL*

Author Manuscript Author Manuscript Author Manuscript Author Manuscript

transcript using Lipofectamine 2000 (Invitrogen) and protein lysate was isolated 72 h post-transfection, followed by immunoblotting for FLAG Tag (Cell Signaling, 8146).

RNA-in situ hybridization (RNA-ISH)—Probe for *MERRICAL* was specially developed to detect mouse MERRICAL (Advanced Cell Diagnostics). Cells or tissues sections were fixed for 2 h in 4% paraformaldehyde and further prepared as described by the manufacturer. *In situ* hybridization was performed using RNAscope 2.5 HD Reagent Kit-Red (Advanced Cell Diagnostics) based on manufacturer's protocol.

Cell fractionation—Cell fractionation was performed to separate cytoplasmic, nuclear, and chromatin components using a nuclear extract kit (Active Motif, 40010) following the manufacturer's protocol. RNA was harvested as described previously and cleaned up using the RNeasy kit (Qiagen). Different protein or RNA contents in the fractions were then estimated by western blotting or RT-qPCR.

Preparation of mouse bone marrow derived macrophages—Bone marrow derived macrophages (BMDM) were obtained according to method described.[5] The mice were euthanized by CO2. The femur and tibia bones were isolated with hair, skin, and most of muscle tissue removed. The bones were cut open, and bone marrow was flushed out with a 21G needle and syringe into cold PBS with 2% FBS. The bone marrow was passed through a 70 μm cell strainer in order to remove bone fragments and other tissue. Ammonium chloride solution was used to lyse red blood cells. The collected bone marrow cells were cultured in Iscove's Modified Dulbecco's Medium (IMDM) supplemented with 10% FBS and 15% filtered L929 cell culture supernatant (containing monocyte-colony stimulating factor, M-CSF). The BMDMs were mature and ready for treatment after 7 days. For M1 (LPS group) activation, BMDMs were treated with 100 ng/mL LPS overnight. To assess the impact of MM102 small molecule inhibitor on the interaction between MLL-WDR5 and subsequent cytokine expression in the presence or absence of LPS, BMDMs were treated with MM102 (S7265, 10uM, Selleck) for 16 h, then treated with 1μM/ml LPS for 0, 4, and 16 h.

RNA isolation and real-time quantitative PCR—Total RNA was extracted by using Trizol reagent following the manufacturer's protocol (15596-026 Invitrogen, MA, USA). The concentration and quality control of RNA was examined using NanoDrop 2000 (Thermo Fisher, MA, USA). cDNA was produced using High-Capacity cDNA Reverse Transcription Kit (4368814, Thermofisher, MA, USA). mRNA expression levels were normalized to b-actin. GoTaq qPCR (A6001, Promega) was used for quantitative real-time PCR analysis with Quantstudio 6 Pro (Thermofisher) following the manufacturer's instructions. A list of primers is presented in Table S1.

Cytokine profiling in the plasma and supernatants—Mouse plasma blood samples were obtained by cardiac puncture during sacrifice, then centrifuged to separate the plasma. For the supernatants from primary $CD4^+$ T cells, $1*10^6$ isolated cells per well were plated in the 24-well plate with Mouse T-Activator CD3/CD28 for T cell expansion and activation (11452D, Gibco, MA, USA) in 1 mL RPMI Media 1640 with 10% FBS and 1%P/S according to the manufacturer's instructions. After culture for 24h, the supernatants

Author Manuscript Author Manuscript Author Manuscript Author Manuscript

were collected and directly subjected for the further experiments. Plasma and supernatants from primary $CD4^+$ T cells were then subjected to Mouse Cytokine/Chemokine 31-Plex Discovery Assay Array (MD31), and TGFβ 3-Plex Discovery Assay Multi Species Array (TGFβ1-3) (Eve Technologies, AB, Canada).

Phagocytosis assay—Assessment of BMDM phagocytic capacity was performed using the Vybrant Phagoctyosis Assay Kit (V6694, Thermofisher). Briefly, BMDMs were transfected with GapmeRs for *MERRICAL* or NS control at 50mM, and seeded into 96-well plates. 100 μL of prepared *E. coli* BioParticle suspension was added to each well, and cells were intubated for 2 h. Following intubation, 100 μL of trypan blue suspension was added to all wells and subsequently aspirated. Fluoroescence was measured using a microplate reader at ~480 nm excitation, ~520- mm emission. Net phagocytosis was subsequently calculated per manufacturer's protocol.

Transwell–cell migration assay—BMDMs were serum starved for 12 h. Cells (1×10^5) were seeded into the 8 μm pore size inserts and induced by supernatant from NS control or *MERRICAL* KD BMDM, and in the absence (IgG) or presence of neutralization antibodies against CCL3 and CCL4 for 16h. Cells were then fixed and stained with DAPI. The bottom sides of the inserts were imaged and quantified by ImageJ software.

Endothelial cell monolayer adhesion assay—bEnd3 cells were seeded in 12-well tissue culture plates. After the endothelial cells reached sub-confluency, they were incubated with supernatant from NS control or *MERRICAL* KD BMDM for 16h. Isolated mouse PBMCs were resuspended and labeled with Calcein AM (Molecular Probes, Eugene, OR, U.S.A.) at 37°C for 45 min. After washing once with Dulbecco's phosphate buffered saline (DPBS), PBMC were added to the bEnd3 cell monolayers and co-cultured for 1h. After washing once with DPBS, fluorescent images were taken using an inverted fluorescence microscope.

Bulk RNA-Seq analysis—RNA-Seq transcriptomic analysis was performed after ribodepletion and library construction by using Illumina performed after ribodepletion and standard library construction using Illumina HiSeq2500 V4 2x150 PE (Genewiz). All samples were processed by using a pipeline published in the bcbio-nextgen project (https://github.com/bcbio/bcbio-nextgen). Raw reads were filtered and examined for quality control through running FastQC (http://www.bioinformatics.babraham.ac.uk/projects/fastqc/) and filtered reads were used to generate library and further analysis. Trimmed reads were aligned to UCSC build mm10 of the mouse genome and augmented with transcript information from Ensembl releases 86 (H. sapiens) using STAR. Total gene hit counts and CPM values were calculated for each gene and downstream differential expression analysis between specified groups was performed using DESeq2 and an adapted DESeq2 algorithm that excludes overlapping reads. Genes with adjusted p value <0.05 and log2fold-change (>0.58) were identified as differentially expressed genes for each comparison. The mean quality score of all samples was 37.21 with a range of 27,963,821-45,892,062 reads per sample. All samples had at least >90% of mapped fragments over total fragments.

Author Manuscript Author Manuscript Author Manuscript Author Manuscript

Pathway enrichment analysis—Differentially expressed genes (DEGs) were identified as having at least 1.5-fold changes and adjusted p values <0.05 (false discovery rate). The DEGs were visualized using hierarchical clustering plot. DEGs were subjected to gene set enrichment analyses by using Ingenuity Pathway Analysis (IPA) software functional annotation tool. The significant values for the canonical pathways were calculated by Fisher exact test. R package GOplot91 was used for visualization of pathway enrichment analysis on the set of DEGs (adjusted P-value < 0.05).

Immunofluorescence staining—For immunofluorescence staining, cells were fixed in 4% PFA (Boston Bio Products) for 24h and embedded in paraffin for sectioning. To characterize atherosclerotic lesions, we embedded the aortic root, and aortic arch in optimal cutting temperature (OCT) compound (Cat#23730571, Fisher Scientific, USA) after harvesting the hearts and aortas. We prepared 7-μm frozen serial sections through the aortic sinus with all three valve leaflets visible, aortic arch with all three branches (left subclavian artery, left common carotid artery, and brachiocephalic artery) visible. For plaque area analysis in aorta, mouse aortas were stained with fresh Oil Red O solution for 2 h at room temperature. The stained aortas were destained with 70% ethanol several times. Serial aortic root sections were stained with oil red O or used for immunostaining to detect vascular smooth muscle cells (VSMCs) (anti-αSMA, 1:500, Sigma-Aldrich, A5228) and macrophages (CD68 (1:100, Abcam, AB201845)). Slide sections were blocked with 5% donkey serum (Jackson ImmunoResearch Lab) for 1 h and then incubated with primary antibodies overnight at 4°C. Slides were washed and incubated with conjugated secondary antibodies (Jackson ImmunoResearch Lab) Cy3 conjugated donkey anti-rat secondary antibody (1:300, Cat#: 712-165-153), Alexa 647 conjugated donkey anti-rabbit secondary antibody (1:300, Cat#: 711-605-152) and Alexa 488 conjugated donkey anti-rabbit secondary antibody (1:300, Cat#: 711-545-152) for 90 min at room temperature. Cell nuclei were stained with 4′,6-diamidino-2-phenylindole (DAPI). Immunofluorescence imaging was performed by BIDMC confocal imaging and IHC core facility. Images were acquired on a Carl Zeiss LSM 880 confocal microscope using Zen black software version 2.3 SP1 (BIDMC confocal imaging and IHC core facility). Objective lenses 10× 0.45 NA and 20x 0.8 NA were used for image acquisition. Lesion areas of aorta roots were defined by the internal elastic lamina to the luminal edge of the lesion. All the evaluations were carried out by two observers in a blind manner.

Optical clearing and 3D light sheet microscopy—Mouse aortas were isolated and fixed in 4% paraformaldehyde overnight at 4°C. iDISCO optical clearing protocol was followed as described elsewhere with modifications.[6] Following the incubation with Alexa Fluor conjugated antibodies - CD31-Alexa Fluor 488 (1:100, Biolegend, 102406), αSMA-Alexa Fluor 594 (1:500, Sigma-Aldrich, A5228) and CD68-Alexa Fluor 647(1:100, Abcam, AB201845), aortas were embedded in 5% agarose in PBS and allowed to cool on ice. Excess agarose was trimmed, and the blocks were subjected to subsequent steps in the protocol until the final incubation and clearing in 100% Dibenzyl ether (DBE). An Ultramicroscope II (LaVision Biotec, Germany) light-sheet microscope at the Harvard Neurobiology Imaging Facility Core was used to image the cleared samples (2x objective lens, 1 × zoom; light-sheet thickness set to 3.89 μm, step size 5 μm). Images were analyzed in Imaris software

Author Manuscript Author Manuscript Author Manuscript Author Manuscript

(Oxford Instruments). Plaques were segmented using the manual surface creation method. Plaque volume was obtained from the surface statistics tab. $CD68^+$ spots within the plaque were visualized by first masking the 647 nm channel using the plaque surface and then employing the spot detection algorithm.

Mononuclear cell preparation and flow cytometry—Mononuclear cells for flow cytometry were isolated from the aorta, PBMC and BMDM to detect the characterization of different cell populations. Mouse aortas were digested by using an optimized digestion enzyme mix recipe (Collagenase I 450U/mL, Collagenase XI 125U/mL, DNase I 60U/mL, Hyaluronidase 60U/mL, and Elastase 50 ng/ml). After that, samples were resuspended to obtain single cell suspensions.[1] BMDMs were digested with cell stripper (Corning 25-056-CI) to single cell suspensions. After preparing the single cell suspension according to the above methods, the samples from were sequentially filtered through 40μm strainers. Following the manufacturer's instructions, appropriately fluorescently labeled antibodies were added at predetermined optimum concentrations and incubated on ice for 20 min in the dark for cell-surface staining. Cells were stained with LIVE/DEAD Cell Stain (Invitrogen), followed by staining for cell surface markers, and then fixed and permeabilized with the Cytofix/Cytoperm kit (554714BD, Biosciences) for intracellular staining. After washing with PBS, centrifuging at 350xg for 5 min, samples were resuspended for flow cytometric analysis (BD FACS Analyzer LSR, or BD FACS Analyzer Symphony). The antibodies for flow cytometry are attached in Table S1. All flow data were analyzed by FlowJo 10.7.1.

Western blot—Cells were lysed in RIPA buffer (ThermoFisher Scientific, USA) containing 1% protease and phosphatase inhibitors and resolved by SDS-PAGE. The proteins were separated by gel electrophoresis and then transferred onto PVDF membranes (Bio-Rad, USA). The membranes were blocked with 5% non-fat milk in 1X TBST at room temperature for 1 h and incubated overnight at 4°C with antibodies against β-actin (3700, 1:2000. Cell Signaling), Histone H3 (tri methyl K4) (ab8580, 1:1000, Abcam), Histone H3 (di methyl K9) (Ab32521, 1:1000, Abcam), and Histone H3K4me2 Polyclonal Antibody (39141, 1:1000, Thermofisher). Membranes were incubated with secondary antibody for 1 h at room temperature. Protein bands were detected by enzyme-linked chemiluminescence using a luminescent image analyzer (Bio-Rad, Chemidoc).

Co-immunoprecipitation (Co-IP)—Co-IP assay of MLL and WDR5 was performed using the Universal Magnetic Co-IP Kit (#54002, Active Motif), according to the manufacturer's protocol. Briefly, BMDMs were transfected with GapmeRs for *MERRICAL* or nonspecific control #1 at 50mM for 48 h, then subsequently treated with LPS (1μM/ml, 4 h) and PBS (vehicle control). Cells were harvested and resuspended in Complete Wholecell Lysis Buffer and incubated at 4°C for 30 min. Part of the cell lysates (10%) was saved as an input sample. The remaining lysate was combined with WDR5 (13105, 3 μg, Cell Signaling), or anti-IgG (2727, 3 μg, Cell Signaling) antibody, along with Co-IP/Wash Buffer at 4°C for 4 h. Protein G Magnetic beads were then added to the mixture, incubated at 4°C for 1 h, and washed with Co-IP/Wash Buffer four times. Each bead pellet was resuspended in 20 μL 2X loading buffer and subjected to western blot for MLL (61295, 1:500, Active Motif) and WDR5 (13105, 1:1000, Cell Signaling).

Author Manuscript Author Manuscript Author Manuscript Author Manuscript

Chromatin immunoprecipitation (ChIP)—ChIP assay was performed according to the manufacturer's protocol from Upstate, using the ChIP assay kit (#9003, Cell signal) with modifications. Briefly, BMDMs were treated with LPS (1μM/ml, 2 h) and PBS (vehicle control). Cells were cross-linked with 1% formaldehyde for 15 min at room temperature, and then the reaction was stopped by incubating in glycine with a final concentration of 0.125 M for 5 min. Cells were washed three times with cold PBS and harvested by scraping with cell scraper. Then the cells were lysed in the SDS lysis buffer (1% SDS, 10 mM EDTA, and 50 mM Tris-HCl, pH 8.1) on ice for 10 min. The samples were sonicated into DNA fragments of 0.2–1 kb (checked by agarose gel electrophoresis/ethidium bromide staining) and microcentrifuged at maximal speed for 10 min at 4°C. The supernatant was precleared by rotating with 60 μl of Salmon Sperm DNA/protein-agarose slurry for 30 min at 4°C and then aliquoted after centrifugation. 20 μl was saved as input and 200 μl (equal to one-fifth the number of cells from one 100% confluent 15-cm dish) was used for each antibody. Each 200 μl supernatant was diluted with 800 μl of ChIP dilution buffer (0.01% SDS, 1.1% Triton X-100, 1.2 mM EDTA, 16.7 mM Tris-HCl, pH 8.1, and 167 mM NaCl) and incubated with the specific antibody (1g/sample) at 4°C overnight. A mock precipitation without antibody was used as negative control. The next day, 60 μl of salmon sperm DNA/protein-agarose slurry was added to each sample and incubated at 4°C for another 2–4 h. The beads were then washed for 3–5 min with 1 mL of each buffers listed: low salt wash buffer (0.1% SDS, 1% Triton X-100, 2 mM EDTA, 20mM Tris-HCl, pH 8.1, 150 mM NaCl), high salt wash buffer (0.1% SDS, 1% Triton X-100, 2 mM EDTA, 20 mM Tris-HCl, pH 8.1, 500 mM NaCl), and LiCl wash buffer (0.25 M LiCl, 1% IGEPAL-CA630, 1% deoxycholic acid (sodium salt), 1 mM EDTA, 10 mM Tris-HCl, pH 8.1). After all washes, pellets were suspended by vortexing with 150 μl of freshly prepared elution buffer (0.1 M NaHCO3, 1% SDS) for 15 min, and then the supernatant was collected. This elution progress was repeated once again, and in total 300 μl elutes were collected. The one-tenth input was diluted with dilution buffer to a total volume of 300 μl. Elutes and diluted inputs were incubated in 0.3 M NaCl at 65°C for 4 h to reverse formaldehyde cross-linking. Then 10 L of 0.5 M EDTA, 20 μl of 1 M Tris-HCl, pH 6.5, and 20 g of proteinase K were added to the sample and incubated at 45°C for 1 h. DNA was extracted with phenol/chloroform and then incubated with 10 g of glycogen in 75% ethanol at 20°C overnight. After precipitation by centrifuging at 12,000 g for 30 min at 4°C, the recovered DNA pellets were dissolved in 30 ml of distilled water. Amplifications were performed using RT qPCR with SYBR Green Master Mix (GoTag PCR system, Promega M7122). The qPCR primers used are attached in Table S1.

RNA-in situ hybridization (RNA-ISH)—Probe for *MERRICAL* was specially developed to detect mouse *MERRICAL* (ENSMUST00000216842.2) (Advanced Cell Diagnostics). Cells or tissues sections were fixed for 2 h in RNAase-free 4% paraformaldehyde and further prepared as described by the manufacturer (Advanced Cell Diagnostics). *In situ* hybridization was performed using RNAscope 2.5 HD Reagent Kit-Red (Advanced Cell Diagnostics) based on manufacturer's protocol.

RNA pull down—Biotin-labeled *MERRICAL* and LacZ were generated *in vitro* using T7 RNA Polymerase transcription kit (Promega) and Biotin RNA Labeling Mix (Roche).

Author Manuscript Author Manuscript Author Manuscript Author Manuscript

The Biotinylated RNA was incubated with 2 μL DNase I at 37°C for 15 min to remove DNA template and then purified using G-50 Sephadex columns (Roche). The nuclear protein was homogenized by 20 strokes using a Dounce homogenizer, followed by centrifuging at 15,000 x g for 15 min at 4°C. The nuclear lysate was pre-cleared by incubating with 60 μL streptavidin agarose beads (Thermo Scientific) at 4°C for 1 h with gentle rotation. The biotinylated RNA was heated to 90°C for 2 min and placed on ice for 2 min to allow proper RNA secondary structure formation. The folded RNA was then added to the pre-cleared nuclear lysate and incubated at 4°C for 2 h. Then 60 μL prewashed streptavidin agarose beads were added to the reaction and rotated at 4°C for 1 h. At the end of incubation, beads were collected by centrifugation at 12,000 x g for 1 min and washed with ice-cold NT2 buffer at 4°C five times. After washing, 40μL 2× Laemmli loading buffer were added to the beads and boiled for 10 min at 100°C. The supernatant was collected and analyzed by western blot.

RNA immunoprecipitation (RIP)—RNA immunoprecipitation (RIP) assays were conducted to confirm *MERRICAL*-H3K4me3 interactions using a Magna RIP Kit (Millipore, 17–700) according to the manufacturer's instructions. Briefly, cells were collected for lysis using RIP lysis buffer containing RIP buffer, a protein inhibitor cocktail and an RNase inhibitor for 10 min on the ice. Part of the cell lysates (10%) was saved as an input sample. The remaining lysates (90%) were diluted with RIP immunoprecipitation buffer and incubated with magnetic beads conjugated to anti-Histone H3 (tri methyl K4) (ab8580, 1:50, Abcam), or anti-IgG (Millipore, PP64B) antibody overnight at 4°C. The beads were washed with RIP wash buffer six times. After washing, 50 μL of the immunoprecipitate was saved for western blot analysis. Immunoprecipitated RNA was extracted by Trizol reagent (Invitrogen, 15596-026), and analyzed by RT-qPCR. RIP assays were also conducted to confirm MERRICAL-WDR5 interactions in the presence of absence of 1μM/ml LPS for 4 h. Briefly, cells were collected for lysis using polysome lysis buffer, a protein inhibitor cocktail, and an RNA inhibitor and incubated overnight at −80°C. Part of the cell lysates (10%) was saved as an input sample. The remaining lysates (90%) were added to magnetic beads resuspended in NET-2 buffer conjugated to WDR5 (13105, 5 μg, Cell Signaling), or anti-IgG (2727, 5 μg, Cell Signaling) antibody overnight at 4°C, after they were washed in NT-2 buffer six times. The resulting immunoprecipitate was washed with NT-2 buffer six times, and resuspended in 150μL proteinase K buffer. Immunoprecipitated RNA was isolated and purified using phenol:chloroform:isoamyl alcohol (125:24:1), chloroform, 5M ammonium acetate, 7.5M LiCl, glycogen, and absolute ethanol, and analyzed by RT-qPCR.

Chromatin Isolation by RNA Purification (ChIRP)—BMDM cells were treated with LPS (1ug/ml, 2h) to induce chemokine expression. The ChIRP assay was performed using crosslinked nuclear extract obtained from approximately 9×10^7 cells, following a previously described protocol. {Chu, 2012 #228} Briefly, the cells were crosslinked with 1% formaldehyde and subsequently lysed using lysis Buffer (50 mM Tris HCl pH = 7, 10 mM EDTA, 1% SDS). The cell extract was then subjected to sonication using a Bioruptor device for 15 cycles (30 s ON/45 s OFF). After sonication, the extract was centrifuged at maximum speed to remove insoluble chromatin. A 1% fraction of the cleared extract was preserved

Author Manuscript Author Manuscript Author Manuscript Author Manuscript

as input, while the remaining material was diluted with Hybridization Buffer (containing 15% formamide, 500 mM NaCl, 1 mM EDTA, 0.5% SDS, and supplemented with protease and RNAse inhibitors). The diluted extract was incubated overnight at room temperature with specific probes, and the mixture was rotated to facilitate probe-target interactions. On the following day, 400 μL of Streptavidin magnetic beads (Dynabeads MyOne Streptavidin C1 - Thermo Fisher) were added to each pulldown condition. The pulldown reactions were then incubated for 4 h at room temperature with rotation. Subsequently, the beads were washed five times with Wash Buffer (composed of 2× saline sodium citrate [SSC] and 0.5% SDS). Elution of the bound material was performed using PK buffer (containing 100 mM NaCl, 1 mM EDTA, 0.5% SDS, and 10 mM Tris HCl [pH 7] or [pH 8] for RNA or DNA elution, respectively). To analyze RNA enrichment, 10% of the ChIRP samples was used for RT-qPCR analysis after standard RNA extraction. For DNA analysis, the remaining material was utilized to amplify promoter region of genes including CCL3, CCL4 and IL-1β by qPCR. The ChIRP assay employed a pool of 20 different biotinylated oligonucleotides as probes to specifically pull down *MERRICAL* RNA. As independent controls, a probe set the negative control, LacZ gene were used. Each reaction utilized a total of 300 p.m. of probe (100 p.m. of each *MERRICAL* probe or 150 p.m. of LacZ biotinylated oligos). *MERRICAL* Biotinylated probes were obtained from LGC Biosearch Technologies and negative control LacZ probes were obtained from Sigma-Aldrich (Magna ChIRP Negative Control Probe Set).

CUT&RUN assay—CUT&RUN Assay (EpiCypher, 14–1408) and subsequent sequencing analyses were utilized to determine the specificity of *MERRICAL*'s targets, according to the manufacturer's instructions. Briefly, BMDMs were transfected with NS control or *MERRICAL* gapmers and treated with LPS (1ug/ml, 2h). 1.5 million cells per replicate were harvested per condition and washed and mixed with concanavalin A beads for 10 min at room temperature. Then, the cell/bead conjugates were resuspended with antibody buffer containing 0.01% digitonin and either 0.5 μg H3K4me3 antibody or IgG negative control antibody, and incubated overnight at 4°C on a nutator. After overnight incubation, the mixture was washed and incubated with CUTANA pA/G-MNase for 10 min at room temperature. The reaction was stopped, the released chromatin fragments were purified using SPRIselect beads, and the DNA was eluted into TE buffer. Library preparation was performed using the NEBNext Ultra II DNA Library Prep Kit (NEB, #E7103), NEBNext Multiplex Oligos for Illumina - Index Primers Set 1 (NEB, #E75335S) and NEBNext Multiplex Oligos for Illumina - Index Primers Set 2 (NEB, #E7500S). Libraries were sent to the Massachusetts General Hospital NextGen Sequencing Core where the samples were quality-checked by TapeStation, pooled, and sequenced using the Illumina NextSeq 2000 50 PE P2 flow cell (Illumina).

CUT&RUN data was performed with the following analytical steps. The paired-end sequencing read FASTQ files for each sample were taken as the input. Trimmomatic v0.36 was used for adapter sequences trimming at the 3′ ends of each read (Bolger et al., 2014) with a two-step trimming process to improve the quality (K-seq). The reads were aligned to the reference mouse mm10 assembly by Bowtie2 v2.5.1 with settings –end-to-end, –very-sensitive, –no-mixed, –no-discordant, –dovetail, -I 10 -X 700 considers mates that overlap

Author Manuscript Author Manuscript Author Manuscript Author Manuscript

with each other, usually when fragment length is less than read length, as a concordant alignment. After alignment, Samtools v1.14 was used to do mapping quality filtering and file format conversion in preparation for further analysis. We used a recent tool called Sparse Enrichment Analysis for CUT&RUN (SEACR v1.3) developed by the Henikoff Lab for the peak calling. The bedGraph files from paired-end sequencing were used as input and peaks were defined as contiguous blocks of base pair coverage that did not overlap with blocks of background signal delineated in the IgG control. Since the fragment counts were normalized with the spike-in read count, the normalization option of SEACR was set to “non”. Finally, the peak calling results from each sample were displayed by the Integrative Genomic Viewer (IGV v2.16).

Study approval—All protocols concerning animal use were approved by the Institutional Animal Care and Use Committee at Brigham and Women’s Hospital and Harvard Medical School, Boston, MA, USA and conducted in accordance with the National Institutes of Health (NIH) Guide for the Care and Use of Laboratory Animals. Animal studies were performed in male Ldlr−/− mice (The Jackson Laboratory).

QUANTIFICATION AND STATISTICAL ANALYSIS

Statistical analyses were performed using GraphPad Prism version 7.0 (GraphPad Software Inc). Student t test was used to determine statistical significance between two groups.[7] ANOVA with Bonferroni’s test was used to determine differences between more than two groups. Data are expressed as mean ± SEM. In all figures *, **, ***, and **** denote $p < 0.05$, 0.025, 0.01, and 0.001 respectively, while no significant difference is abbreviated “ns”.

Supplementary Material

Refer to Web version on PubMed Central for supplementary material.

ACKNOWLEDGMENTS

The authors wish to acknowledge the Neurophysiology Imaging Facility core at Harvard Medical School (HMS/BCH Center for Neuroscience Research NS072030) and Dr. Philip Cole, Division of Genetics, Brigham and Women’s Hospital, Harvard Medical School, for helpful suggestions. This work was supported by the National Institutes of Health (HL115141, HL134849, HL148207, HL148355, HL171239, and HL153356 to M.W.F.), the American Heart Association (18SFRN33900144 and 20SFRN35200163 to M.W.F), a Harvard-Longwood Research Training in Vascular Surgery NIH T32 grant (5T32HL007734-22 to W.W.), and a postdoctoral fellowship award (826614 to K.L.).

REFERENCES

1. Al-Lawati JA (2017). Diabetes mellitus: a local and global public health emergency!. Oman Med. J 32, 177–179. [PubMed: 28584596]
2. Kaur J. (2014). A comprehensive review on metabolic syndrome. Cardiol. Res. Pract 2014.
3. Zhang Y, Sun X, Icli B, and Feinberg MW (2017). Emerging roles for microRNAs in diabetic microvascular disease: novel targets for therapy. Endocr. Rev 38, 145–168. [PubMed: 28323921]
4. Tabas I, and Bornfeldt KE (2016). Macrophage phenotype and function in different stages of atherosclerosis. Circ. Res 118, 653–667. [PubMed: 26892964]
5. Moore KJ, Sheedy FJ, and Fisher EA (2013). Macrophages in atherosclerosis: a dynamic balance. Nat. Rev. Immunol 13, 709–721.

Author Manuscript Author Manuscript Author Manuscript Author Manuscript

6. Moore KJ, and Tabas I (2011). Macrophages in the pathogenesis of atherosclerosis. Cell 145, 341–355.
7. Hilgendorf I, Swirski FK, and Robbins CS (2015). Monocyte fate in atherosclerosis. Arterioscler. Thromb. Vasc. Biol 35, 272–279. [PubMed: 25538208]
8. Djebali S, Davis CA, Merkel A, Dobin A, Lassmann T, Mortazavi A, Tanzer A, Lagarde J, Lin W, Schlesinger F, et al. (2012). Landscape of transcription in human cells. Nature 489, 101–108.
9. ENCODE Project Consortium (2012). An integrated encyclopedia of DNA elements in the human genome. Nature 489, 57–74.
10. Wang KC, and Chang HY (2011). Molecular mechanisms of long non-coding RNAs. Mol. Cell 43, 904–914.
11. Consortium RGSP (2004). Genome sequence of the Brown Norway rat yields insights into mammalian evolution. Nature 428, 493.
12. Hangauer MJ, Vaughn IW, and McManus MT (2013). Pervasive transcription of the human genome produces thousands of previously unidentified long intergenic noncoding RNAs. PLoS Genet. 9, e1003569.
13. Mattick JS, and Rinn JL (2015). Discovery and annotation of long non-coding RNAs. Nat. Struct. Mol. Biol 22, 5–7.
14. Rinn JL, and Chang HY (2012). Genome regulation by long noncoding RNAs. Annu. Rev. Biochem 81, 145–166. [PubMed: 22663078]
15. Haemmig S, Yang D, Sun X, Das D, Ghaffari S, Molinaro R, Chen L, Deng Y, Freeman D, Moullan N, et al. (2020). Long noncoding RNA SNHG12 integrates a DNA-PK–mediated DNA damage response and vascular senescence. Sci. Transl. Med 12, eaaw1868.
16. Simion V, Zhou H, Haemmig S, Pierce JB, Mendes S, Tesmenitsky Y, Pérez-Cremades D, Lee JF, Chen AF, Ronda N, et al. (2020). A macrophage-specific lncRNA regulates apoptosis and atherosclerosis by tethering HuR in the nucleus. Nat. Commun 11, 6135–6216.
17. Simion V, Zhou H, Pierce JB,Yang D, Haemmig S, Tesmenitsky Y, Sukhova G, Stone PH, Libby P, and Feinberg MW (2020). LncRNA VINAS regulates atherosclerosis by modulating NF-κB and MAPK signaling. JCI insight 5, e140627. [PubMed: 33021969]
18. Shihabudeen Haider Ali MS, Cheng X, Moran M, Haemmig S, Naldrett MJ, Alvarez S, Feinberg MW, and Sun X (2019). LncRNA Meg3 protects endothelial function by regulating the DNA damage response. Nucleic Acids Res. 47, 1505–1522.
19. Zhou H, Simion V, Pierce JB, Haemmig S, Chen AF, and Feinberg MW (2021). LncRNA-MAP3K4 regulates vascular inflammation through the p38 MAPK signaling pathway and cis-modulation of MAP3K4. Faseb. J 35, e21133. [PubMed: 33184917]
20. Ni H, Haemmig S, Deng Y, Chen J, Simion V, Yang D, Sukhova G, Shvartz E, Wara AKMK, Cheng HS, et al. (2021). A Smooth Muscle Cell–Enriched Long Noncoding RNA Regulates Cell Plasticity and Atherosclerosis by Interacting With Serum Response Factor. Arterioscler. Thromb. Vasc. Biol 41, 2399–2416. [PubMed: 34289702]
21. Josefs T, and Boon RA (2020). The long non-coding road to atherosclerosis. Curr. Atheroscler. Rep 22. 55–12. [PubMed: 32772181]
22. Li H, Zhu H, and Ge J (2016). Long noncoding RNA: recent updates in atherosclerosis. Int. J. Biol. Sci 12, 898–910. [PubMed: 27314829]
23. Fernández-Ruiz I. (2018). A new role for lncRNAs in atherosclerosis. Nat. Rev. Cardiol 15, 195. [PubMed: 29493569]
24. Zhang Z, Salisbury D, and Sallam T (2018). Long noncoding RNAs in atherosclerosis: JACC review topic of the week. J. Am. Coll. Cardiol 72, 2380–2390. [PubMed: 30384894]
25. Rinn JL, and Chang HY (2020). Long noncoding RNAs: molecular modalities to organismal functions. Annu. Rev. Biochem 89, 283–308. [PubMed: 32569523]
26. Marchese FP, Raimondi I, and Huarte M (2017). The multidimensional mechanisms of long noncoding RNA function. Genome Biol. 18, 206–213.
27. Engreitz JM, Haines JE, Perez EM, Munson G, Chen J, Kane M, McDonel PE, Guttman M, and Lander ES (2016). Local regulation of gene expression by lncRNA promoters, transcription and splicing. Nature 539, 452–455. [PubMed: 27783602]

Author Manuscript Author Manuscript Author Manuscript Author Manuscript

28. Khyzha N, Khor M, DiStefano PV, Wang L, Matic L, Hedin U, Wilson MD, Maegdefessel L, and Fish JE (2019). Regulation of CCL2 expression in human vascular endothelial cells by a neighboring divergently transcribed long noncoding RNA. Proc. Natl. Acad. Sci. USA 116, 16410–16419. [PubMed: 31350345]
29. Liu S, Liu J, Yang X, Jiang M, Wang Q, Zhang L, Ma Y, Shen Z, Tian Z, and Cao X (2021). Cis-acting lnc-Cxcl2 restrains neutrophil-mediated lung inflammation by inhibiting epithelial cell CXCL2 expression in virus infection. Proc. Natl. Acad. Sci. USA 118, e2108276118.
30. Bornfeldt KE (2022). 2021 George Lyman Duff Memorial Lecture: The Remnant Lipoprotein Hypothesis of Diabetes-Associated Cardiovascular Disease. Arterioscler. Thromb. Vasc. Biol 42, 819–830. 10.1161/ATVBAHA.1122.317163.
31. Goldberg IJ, Isaacs A, Sehayek E, Breslow JL, and Huang L-S (2004). Effects of streptozotocin-induced diabetes in apolipoprotein AI deficient mice. Atherosclerosis 172, 47–53.
32. Srinivasan K, Viswanad B, Asrat L, Kaul CL, and Ramarao P (2005). Combination of high-fat diet-fed and low-dose streptozotocin-treated rat: a model for type 2 diabetes and pharmacological screening. Pharmacol. Res 52, 313–320. [PubMed: 15979893]
33. Collins AR, Meehan WP, Kintscher U, Jackson S, Wakino S, Noh G, Palinski W, Hsueh WA, and Law RE (2001). Troglitazone inhibits formation of early atherosclerotic lesions in diabetic and nondiabetic low density lipoprotein receptor–deficient mice. Arterioscler. Thromb. Vasc. Biol 21, 365–371.
34. Neuhofer A, Wernly B, Leitner L, Sarabi A, Sommer NG, Staffler G, Zeyda M, and Stulnig TM (2014). An accelerated mouse model for atherosclerosis and adipose tissue inflammation. Cardiovasc. Diabetol 13. 23–12. [PubMed: 24438079]
35. Statello L, Guo C-J, Chen L-L, and Huarte M (2021). Gene regulation by long non-coding RNAs and its biological functions. Nat. Rev. Mol. Cell Biol 22, 96–118.
36. Liu T, Porter J, Zhao C, Zhu H, Wang N, Sun Z, Mo Y-Y, and Wang Z (2019). TADKB: Family classification and a knowledge base of topologically associating domains. BMC Genom. 20. 217–17.
37. Chang T-T, Yang H-Y, Chen C, and Chen J-W (2020). CCL4 inhibition in atherosclerosis: effects on plaque stability, endothelial cell adhesiveness, and macrophages activation. Int. J. Mol. Sci 21, 6567. [PubMed: 32911750]
38. Bell RD, Long X, Lin M, Bergmann JH, Nanda V, Cowan SL, Zhou Q, Han Y, Spector DL, Zheng D, and Miano JM (2014). Identification and initial functional characterization of a human vascular cell–enriched long noncoding RNA. Arterioscler. Thromb. Vasc. Biol 34, 1249–1259. [PubMed: 24578380]
39. Haemmig S, and Feinberg MW (2017). Targeting LncRNAs in cardiovascular disease: options and expeditions. Circ. Res 120, 620–623. [PubMed: 28209793]
40. Chen J, Zhuang R, Cheng HS, Jamaiyar A, Assa C, McCoy M, Rawal S, Pérez-Cremades D, and Feinberg MW (2022). Isolation and culture of murine aortic cells and RNA isolation of aortic intima and media: Rapid and optimized approaches for atherosclerosis research. Atherosclerosis 347, 39–46. 10.1016/j.atherosclerosis.2022.03.011. [PubMed: 35306416]
41. Arun G, Aggarwal D, and Spector DL (2020). MALAT1 long non-coding RNA: Functional implications. Noncoding. RNA 6, 22. [PubMed: 32503170]
42. Chen J, Ke S, Zhong L, Wu J, Tseng A, Morpurgo B, Golovko A, Wang G, Cai JJ, Ma X, et al. (2018). Long noncoding RNA MALAT1 regulates generation of reactive oxygen species and the insulin responses in male mice. Biochem. Pharmacol 152, 94–103. [PubMed: 29577871]
43. Dong K, Shen J, He X, Hu G, Wang L, Osman I, Bunting KM, Dixon-Melvin R, Zheng Z, Xin H, et al. (2021). CARMN Is an Evolutionarily Conserved Smooth Muscle Cell–Specific LncRNA That Maintains Contractile Phenotype by Binding Myocardin. Circulation 144, 1856–1875. [PubMed: 34694145]
44. Walter W, Sánchez-Cabo F, and Ricote M (2015). GOplot: an R package for visually combining expression data with functional analysis. Bioinformatics 31, 2912–2914. [PubMed: 25964631]
45. Sachithanandan N, Graham KL, Galic S, Honeyman JE, Fynch SL, Hewitt KA, Steinberg GR, and Kay TW (2011). Macrophage deletion of SOCS1 increases sensitivity to LPS and palmitic

Author Manuscript Author Manuscript Author Manuscript Author Manuscript

acid and results in systemic inflammation and hepatic insulin resistance. Diabetes 60, 2023–2031. [PubMed: 21646388]

46. Saraswathi V, Kumar N, Gopal T, Bhatt S, Ai W, Ma C, Talmon GA, and Desouza C (2020). Lauric acid versus palmitic acid: effects on adipose tissue inflammation, insulin resistance, and non-alcoholic fatty liver disease in obesity. Biology 9, 346.
47. Wang KC,Yang YW, Liu B, Sanyal A, Corces-Zimmerman R, Chen Y, Lajoie BR, Protacio A, Flynn RA, Gupta RA, et al. (2011). A long noncoding RNA maintains active chromatin to coordinate homeotic gene expression. Nature 472, 120–124. [PubMed: 21423168]
48. Li H, Ilin S, Wang W, Duncan EM, Wysocka J, Allis CD, and Patel DJ (2006). Molecular basis for site-specific read-out of histone H3K4me3 by the BPTF PHD finger of NURF. Nature 442, 91–95. [PubMed: 16728978]
49. Chervona Y, and Costa M (2012). The control of histone methylation and gene expression by oxidative stress, hypoxia, and metals. Free Radic. Biol. Med 53, 1041–1047.
50. Russ BE, Olshanksy M, Smallwood HS, Li J, Denton AE, Prier JE, Stock AT, Croom HA, Cullen JG, Nguyen MLT, et al. (2014). Mapping histone methylation dynamics during virus-specific CD8+ T cell differentiation in response to infection. Immunity 41, 853–865.
51. Russ BE, Olshanksy M, Smallwood HS, Li J, Denton AE, Prier JE, Stock AT, Croom HA, Cullen JG, Nguyen MLT, et al. (2014). Distinct epigenetic signatures delineate transcriptional programs during virus-specific CD8+ T cell differentiation. Immunity 41, 853–865.
52. Gomez JA, Wapinski OL, Yang YW, Bureau J-F, Gopinath S, Monack DM, Chang HY, Brahic M, and Kirkegaard K (2013). The NeST long ncRNA controls microbial susceptibility and epigenetic activation of the interferon-γ locus. Cell 152, 743–754.
53. Fanucchi S, Fok ET, Dalla E, Shibayama Y, Börner K, Chang EY, Stoychev S, Imakaev M, Grimm D, Wang KC, et al. (2019). Immune genes are primed for robust transcription by proximal long noncoding RNAs located in nuclear compartments. Nat. Genet 51, 138–150. [PubMed: 30531872]
54. Skene PJ, and Henikoff S (2017). An efficient targeted nuclease strategy for high-resolution mapping of DNA binding sites. Elife 6, e21856. 10.7554/eLife.21856. [PubMed: 28079019]
55. Wang X, Zhu K, Li S, Liao Y, Du R, Zhang X, Shu H-B, Guo A-Y, Li L, and Wu M (2012). MLL1, a H3K4 methyltransferase, regulates the TNFα-stimulated activation of genes downstream of NF-κB. J. Cell Sci 125, 4058–4066. [PubMed: 22623725]
56. Cao F, Townsend EC, Karatas H, Xu J, Li L, Lee S, Liu L, Chen Y, Ouillette P, Zhu J, et al. (2014). Targeting MLL1 H3K4 methyltransferase activity in mixed-lineage leukemia. Mol. Cell 53, 247–261. [PubMed: 24389101]
57. Muppirala UK, Honavar VG, and Dobbs D (2011). Predicting RNA-protein interactions using only sequence information. BMC Bioinf. 12, 489–499. 10.1186/1471-2105-12-489.
58. MacRitchie N, and Maffia P (2021). Light sheet fluorescence microscopy for quantitative three-dimensional imaging of vascular remodelling. Cardiovasc. Res 117, 348–350. [PubMed: 32386306]
59. Palazzo AF, and Lee ES (2015). Non-coding RNA: what is functional and what is junk? Front. Genet 6, 2. [PubMed: 25674102]
60. Nagano T, Mitchell JA, Sanz LA, Pauler FM, Ferguson-Smith AC, Feil R, and Fraser P (2008). The Air noncoding RNA epigenetically silences transcription by targeting G9a to chromatin. Science 322, 1717–1720. [PubMed: 18988810]
61. Ørom UA, Derrien T, Beringer M, Gumireddy K, Gardini A, Bussotti G, Lai F, Zytnicki M, Notredame C, Huang Q, et al. (2010). Long non-coding RNAs with enhancer-like function in human cells. Cell 143, 46–58. [PubMed: 20887892]
62. Guil S, and Esteller M (2012). Cis-acting noncoding RNAs: friends and foes. Nat. Struct. Mol. Biol 19, 1068–1075. [PubMed: 23132386]
63. Ebisuya M, Yamamoto T, Nakajima M, and Nishida E (2008). Ripples from neighbouring transcription. Nat. Cell Biol 10, 1106–1113. [PubMed: 19160492]
64. Dixon JR, Selvaraj S, Yue F, Kim A, Li Y, Shen Y, Hu M, Liu JS, and Ren B (2012). Topological domains in mammalian genomes identified by analysis of chromatin interactions. Nature 485, 376–380.

Author Manuscript Author Manuscript Author Manuscript Author Manuscript

65. Kopp F, and Mendell JT (2018). Functional classification and experimental dissection of long noncoding RNAs. Cell 172, 393–407. [PubMed: 29373828]

66. Bridges MC, Daulagala AC, and Kourtidis A (2021). LNCcation: lncRNA localization and function. J. Cell Biol 220, e202009045. [PubMed: 33464299]

67. Wang H, Fan Z, Shliaha PV, Miele M, Hendrickson RC, Jiang X, and Helin K (2023). H3K4me3 regulates RNA polymerase II promoter-proximal pause-release. Nature 615, 339–348.

68. Livi CM, Klus P, Delli Ponti R, and Tartaglia GG (2016). catRAPID signature: identification of ribonucleoproteins and RNA-binding regions. Bioinformatics 32, 773–775. 10.1093/bioinformatics/btv629.

69. Hirota K, Miyoshi T, Kugou K, Hoffman CS, Shibata T, and Ohta K (2008). Stepwise chromatin remodelling by a cascade of transcription initiation of non-coding RNAs. Nature 456, 130–134. [PubMed: 18820678]

70. Anderson KM, Anderson DM, McAnally JR, Shelton JM, Bassel-Duby R, and Olson EN (2016). Transcription of the non-coding RNA upperhand controls Hand2 expression and heart development. Nature 539, 433–436.

71. de Jager SCA, Bot I, Kraaijeveld AO, Korporaal SJA, Bot M, van Santbrink PJ, van Berkel TJC, Kuiper J, and Biessen EAL (2013). Leukocyte-specific CCL3 deficiency inhibits atherosclerotic lesion development by affecting neutrophil accumulation. Arterioscler. Thromb. Vasc. Biol 33, e75–e83. 10.1161/ATVBAHA.112.300857. [PubMed: 23288165]

Author Manuscript Author Manuscript Author Manuscript Author Manuscript

Highlights

- Macrophage-enriched lncRNA *MERRICAL* increased in diabetes-associated atherosclerosis
- *MERRICAL* in *cis* regulated chemokines CCL3 and CCL4 by guiding WDR5-MLL1 and H3K4me3
- *MERRICAL* KD macrophages had reduced CCL3 and CCL4 expression and chemotactic responses
- *MERRICAL* KD abrogated pro-inflammatory macrophage recruitment and lesion formation

Author Manuscript
Author Manuscript
Author Manuscript
Author Manuscript

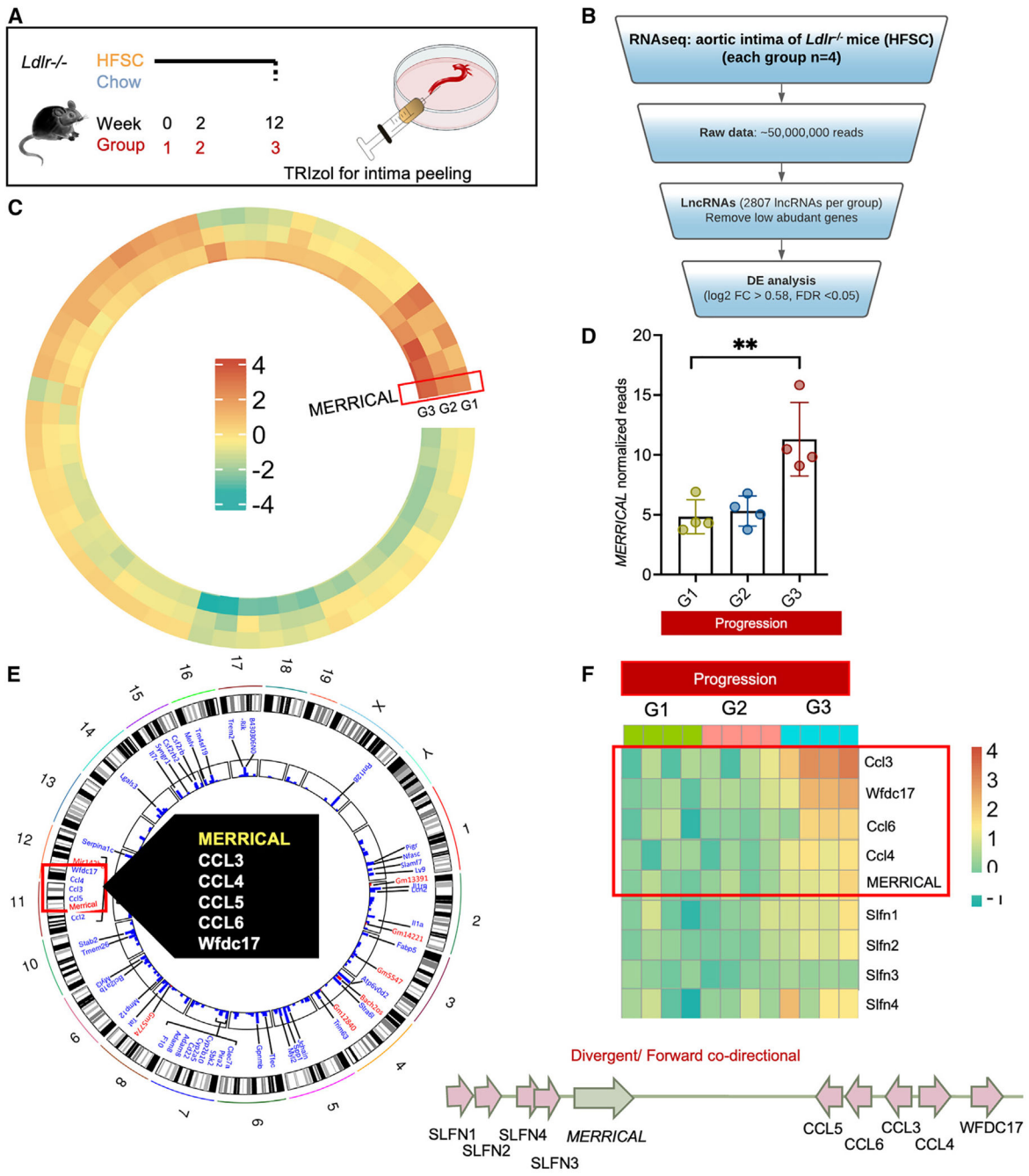

Figure 1. The lncRNA *MERRICAL* is coordinately regulated with a group of chemokine genes during HFSC diet-induced atherosclerosis in mice

(A) RNA derived from the aortic intima of *Ldlr*$^{-/-}$ mice (n = 4, each sample represents RNA pooled from two mice) placed on a high-fat, high-sucrose-containing (HFSC) diet for 0 weeks (group 1), 2 weeks (group 2), or 12 weeks (group 3).

(B) Workflow of genome-wide RNA-seq profiling for the identification of DE lncRNAs (log2 fold change [FC] > 1.5, FDR < 0.05).

(C) Radial heatmap showing the expression of the top 50 significantly regulated lncRNAs during the progression of atherosclerosis induced by the HFSC diet in *Ldlr*$^{-/-}$ mice.

Author Manuscript Author Manuscript Author Manuscript Author Manuscript

(D) Normalized reads from RNA-seq of the lncRNA *MERRICAL* in the aortic intima over atherosclerosis progression.
(E) Circos plot of DE mRNA in G3 vs. G1 (black) paired with DE lncRNA in G3 vs. G1 (red).
(F) Heatmap showing the expression pattern ofthe lncRNA *MERRICAL* and its neighbor genes in the progression phase of diabetes-associated atherosclerosis. Values are mean ± SD. Significance was determined by two-tailed Student's t test. *$p < 0.05$, **$p < 0.01$, ***$p < 0.001$.

Author Manuscript Author Manuscript Author Manuscript Author Manuscript

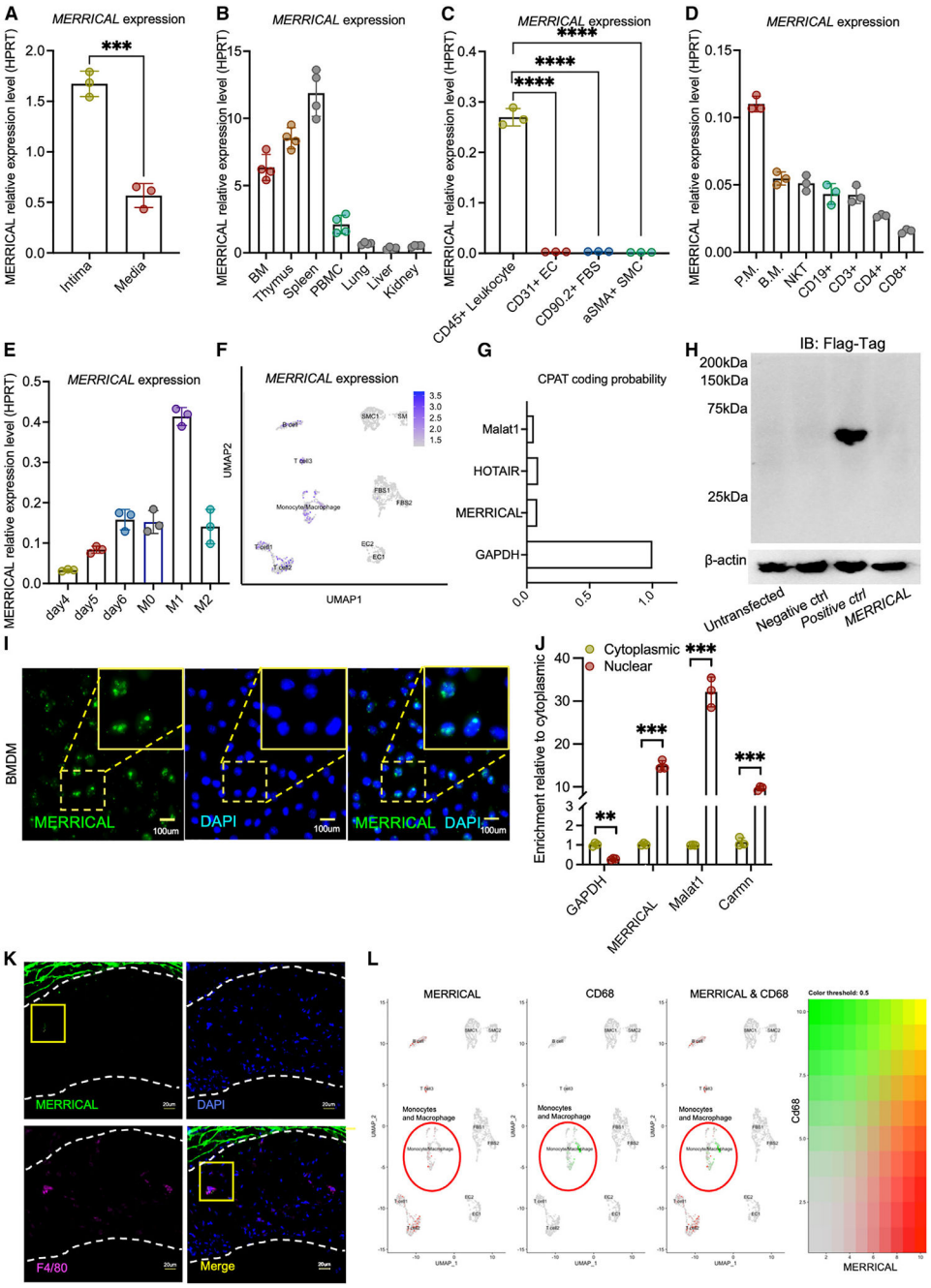

Figure 2. Identification of the lncRNA *MERRICAL* in lesional intima

(A) Quantitative real-time PCR expression analysis for the lncRNA *MERRICAL* in the aortic intima and media in *Ldlr*$^{-/-}$ mice on the HFSC diet for 12 weeks (n = 3).

(B) Quantitative real-time PCR expression analysis of the lncRNA *MERRICAL* in different body organs in 12-week-old C57BL/6 mice (n = 4).

(C) Quantitative real-time PCR expression analysis of the lncRNA *MERRICAL* in different aortic cell types isolated by magnetic beads (CD45^{+} leukocytes, CD31^{+} endothelial cells, CD90.2^{+} fibroblasts, and aSMA^{+} SMCs) from C57BL/6 mice (n = 3).

Author Manuscript Author Manuscript Author Manuscript Author Manuscript

(D) lncRNA *MERRICAL* expression in different types of immune cells isolated from C57BL/5 mice. P.M, peritoneal macrophages; B.M, BMDMs; NKT, natural killer T cells; $CD19^+$, B cells; $CD3^+$, total T cells; $CD4^+$, $CD4^+$ T cells; $CD8^+$, cytotoxic T cells; (n = 3).
(E) LncRNA *MERRICAL* expression kinetics in macrophages differentiated from BM isolated from C57BL/6 mice (n = 3).
(F) Uniform manifold approximation and projection (UMAP) of expression of the lncRNA *MERRICAL* in different aortic cell types after aortic single-cell RNA-seq.
(G) The coding potential assessment tool (CPAT) predicts very low coding potential for the lncRNA *MERRICAL*.
(H) To test the coding potential, the *MERRICAL* sequence was cloned upstream of the 3 × FLAG tag cassette, transfected in HEK293T cells, and immunoblotted for FLAG antibody. A positive control was provided with the kit (n = 3 experiments).
(I) RNA-ISH for negative control and *MERRICAL* probes on PFA-fixed BM-derived macrophages (BMDMs).
(J) Quantitative real-time PCR analysis for RNA derived from BMDMs, separated into cytoplasmic and nuclear fractions and normalized to the cytoplasmic fraction (n = 3).
(K) Representative image of *MERRICAL* (cyan dots) colocalized with $F4/80^+$ macrophages (pink) in mouse aortic lesions of $Ldlr^{-/-}$ mice fed the HFSC diet.
(L) Heatmap showing *MERRICAL* (red) and Cd68 (green) co-expression in the single-cell transcriptome analysis of RNA from the descending aorta of $Ldlr^{-/-}$ mice fed the HFSC diet. Scale bars, 200 μm. Values are mean ± SD. Significance was determined by two-tailed Student's t test. *p < 0.05, **p < 0.01, ***p < 0.001.

Author Manuscript Author Manuscript Author Manuscript Author Manuscript

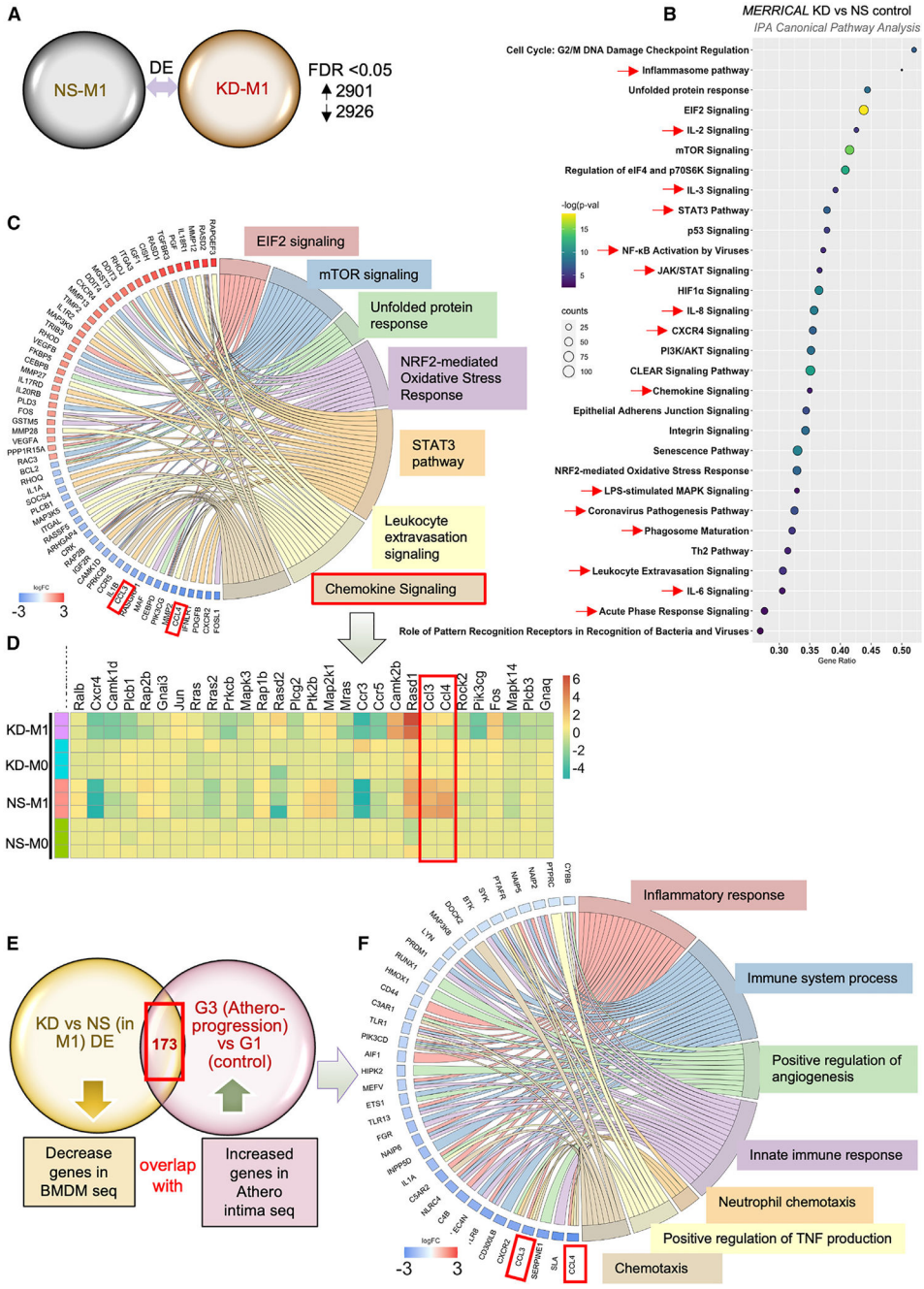

Figure 3. *MERRICAL*-deficient macrophages inhibit pro-inflammatory responses and chemokine CCL3/CCL4 expression *in vitro*

(A) Differential expression analysis using DEseq2 was applied to compare non-specific (NS) control gapmeR-treated BMDMs (M1 phase) with the *MERRICAL* gapmeR knockdown (KD) BMDMs (M1 phase).

(B) IPA canonical pathway analysis from DEGs of *MERRICAL* KD BMDMs compared with NS controls.

Author Manuscript Author Manuscript Author Manuscript Author Manuscript

(C) GOChord plot showing the significantly regulated genes (log2 FC > 3, FDR < 0.05) involved in the top 7 enriched pathways when comparing *MERRICAL* KD BMDMs with NS controls.

(D) Heatmap showing significantly regulated genes in the chemokine signaling pathway.

(E) Overlap of significantly downregulated genes (from comparison of *MERRICAL* KD BMDMs with NS controls) with significantly upregulated genes (from aortic intimal RNA-seq of $Ldlr^{-/-}$ mice fed the HFSC diet, G3 progression versus control).

(F) GOChord plot showing overlapping genes in (E) (log2 FC > 0.58, FDR < 0.05) involved in the top 7 enriched pathways.

Author Manuscript Author Manuscript Author Manuscript Author Manuscript

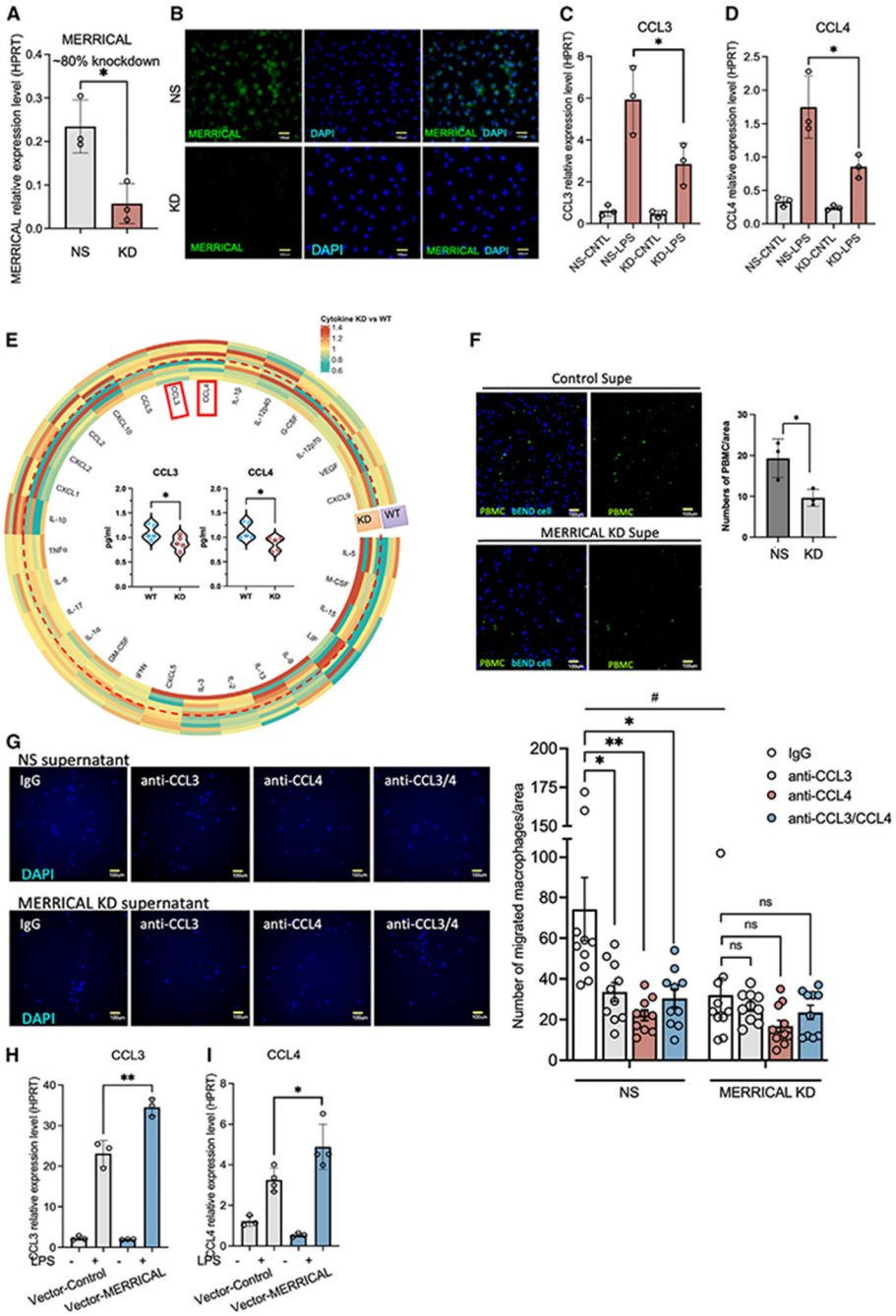

Figure 4. Loss and gain of function of the lncRNA *MERRICAL* regulating chemotaxis and pro-inflammatory response *in vitro*

(A) Quantitative real-time PCR analysis of KD efficiency using gapmeR targeting the lncRNA *MERRICAL* in BMDMs.

(B) RNA-ISH confirmed *MERRICAL* KD in BMDMs.

(C and D) Quantitative real-time PCR analysis confirmed the CCL3 and CCL4 expression in NS control and *MERRICAL* KD BMDMs.

(E) Radial heatmap showing cytokine array in supernatant from NS control and *MERRICAL* BMDMs.

Author Manuscript Author Manuscript Author Manuscript Author Manuscript

(F) Immunofluorescence imaging of representative fields of the PBMC adhesion assay on the bEnd.3 cell monolayer cultured for 24 h with supernatant from NS control or *MERRICAL* KD BMDMs. Scale bars, 100 μm.

(G) Immunofluorescence imaging of representative fields of BMDMs migrated through the Transwell filter with the supernatant of NS control or *MERRICAL* KD BMDMs, supplemented with the neutralization antibody anti-CCL3 and CCL4 loaded in the lower chamber.

(H and I) CCL3 and CCL4 mRNA expression in control vector- or *MERRICAL* overexpression vector-treated BMDMs.

Values are mean ± SD. Significance was determined by two-tailed Student's t test for (C)–(F) and (H). Significance was determined by two-way ANOVA for (G). *$p < 0.05$, **$p < 0.01$, ***$p < 0.001$.

Author Manuscript Author Manuscript Author Manuscript Author Manuscript

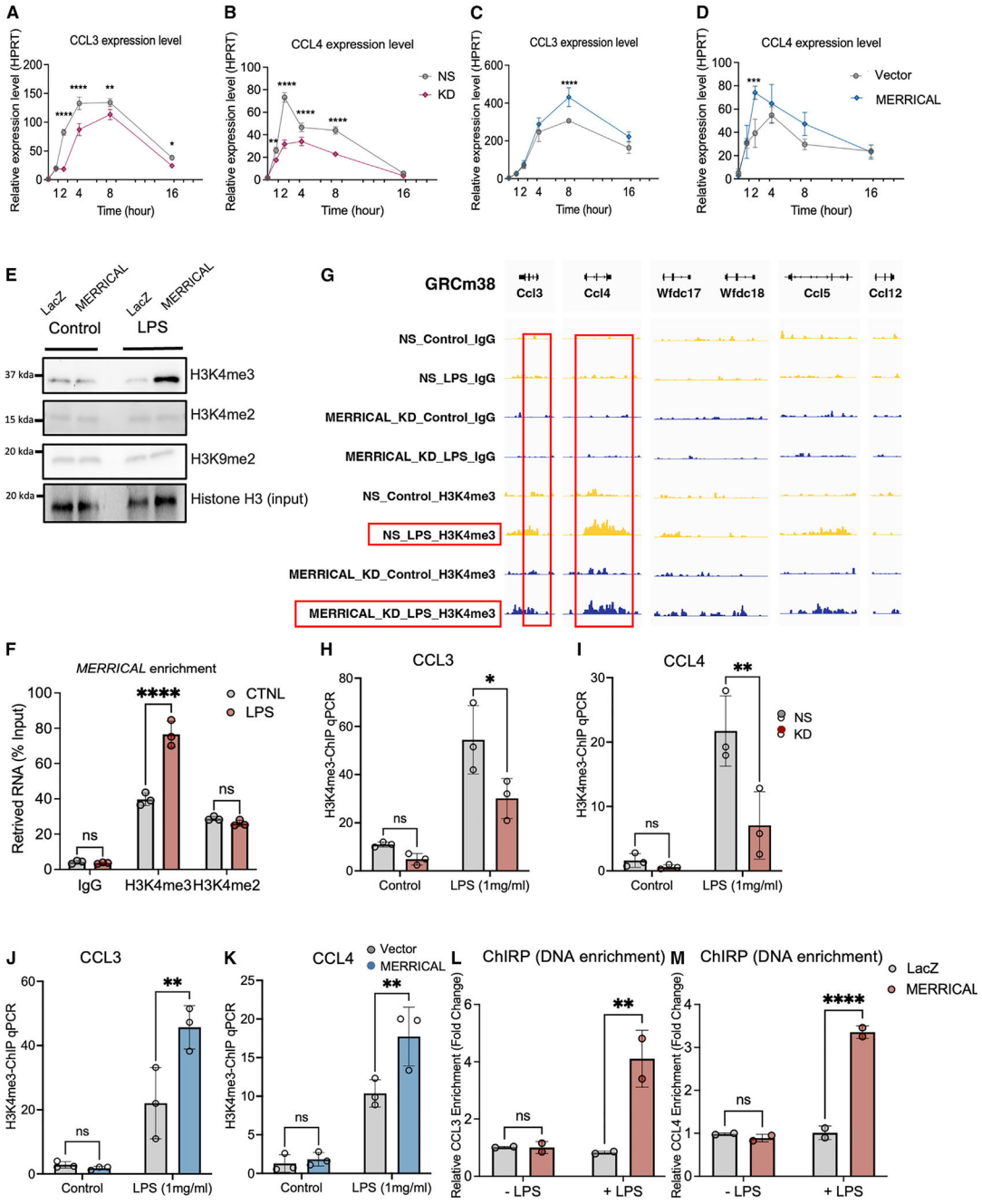

Figure 5. The lncRNA *MERRICAL* regulates CCL3 and CCL4 transcription through interaction with H3K4me3

(A–D) Quantitative real-time PCR analysis of CCL3 and CCL4 expression in BMDMs transfected with NS gapmeR (NS), *MERRICAL* gapmeR (KD), pcDNA3.1-vector (vector), and pcDNA3.1-*MERRICAL* overexpression (*MERRICAL*) in a time-dependent manner (n = 3).

(E) Biotinylated lncRNA pull-down using wild-type (lacZ) or *MERRICAL* in BMDM nuclear lysates from a control or an LPS (1 μg/mL, 2 h) (n = 3).

Author Manuscript Author Manuscript Author Manuscript Author Manuscript

(F) RNA immunoprecipitation (RIP) followed by qRT-PCR analysis of co-purified RNAs in BMDMs.

(G) Genomic snapshot showing CUT&RUN signals for H3K4me3 and IgG for Ccl3, Ccl4, Wdfc17, Wfdc18, Ccl5, and Ccl12 from both NS and MERRICAL KD groups with or without LPS treatment (2 h).

(H–K) ChIP-qPCR analysis of H3K4me3 in BMDMs transfected with NS gapmeR (NS), *MERRICAL* gapmeR (KD), pcDNA3.1-vector (vector), and pcDNA3.1-*MERRICAL* overexpression (*MERRICAL*)

(L and M) DNA enrichment in ChIRP experiments with control (LacZ) and *MERRICAL* probes determined by qPCR and calculated as percentage of input with the indicated primer sets (CCL3 and CCL4).

Values are mean ± SD. Significance was determined by two-tailed Student's t test for (A)–(D) and (F)–(M). *$p < 0.05$, **$p < 0.01$, ***$p < 0.001$.

Author Manuscript Author Manuscript Author Manuscript Author Manuscript

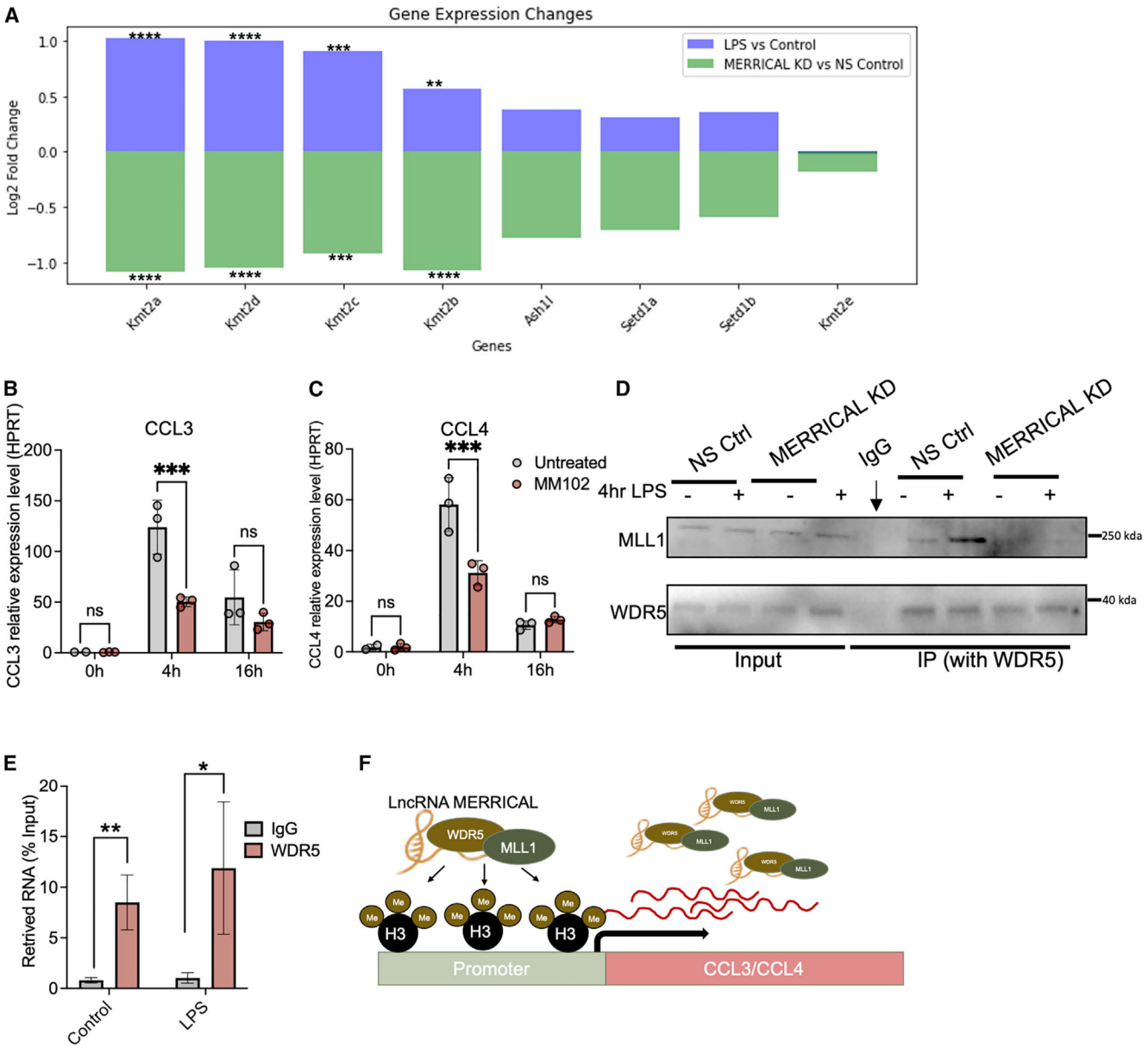

Figure 6. *MERRICAL* interacted with the WDR5-MLL1 complex and facilitated the H4K4me3 modification at the promoter region of CCL3 and CCL4

(A) Bar plot showing H3K4 methylation mediators, including Kmt (MLL) families, and Ashk1, Setd1a, and Setd1b regulation in response to LPS-treated BMDMs (blue bar) and in response to *MERRICAL* KD in BMDMs (green bar) from the RNA-seq analysis.

(B and C) Quantitative real-time PCR analysis of CCL3 and CCL4 expression in BMDMs treated with MM102 (10 μM) with LPS stimulation (1 μM; 0, 4, and 16 h).

(D) IP of WDR5 in both NS control and *MERRICAL* KD BMDMs treated with LPS (4 h), followed by western blotting, which shows interaction between WDR5 and MLL1 under NS control and *MERRICAL* KD conditions in BMDMs.

(E) RIP by IgG or WDR5, followed by qRT-PCR analysis of co-purified RNAs in BMDMs.

Author Manuscript Author Manuscript Author Manuscript Author Manuscript

(F) Illustration showing *MERRICAL* binding with the WDR5-MLL1 complex and facilitating H3K4me3 deposition on the promoter region of CCL3 and CCL4.

Values are mean ± SD. Significance was determined by two-tailed Student's t test for (A)–(E). *$p < 0.05$, **$p < 0.01$, ***$p < 0.001$.

Author Manuscript Author Manuscript Author Manuscript Author Manuscript

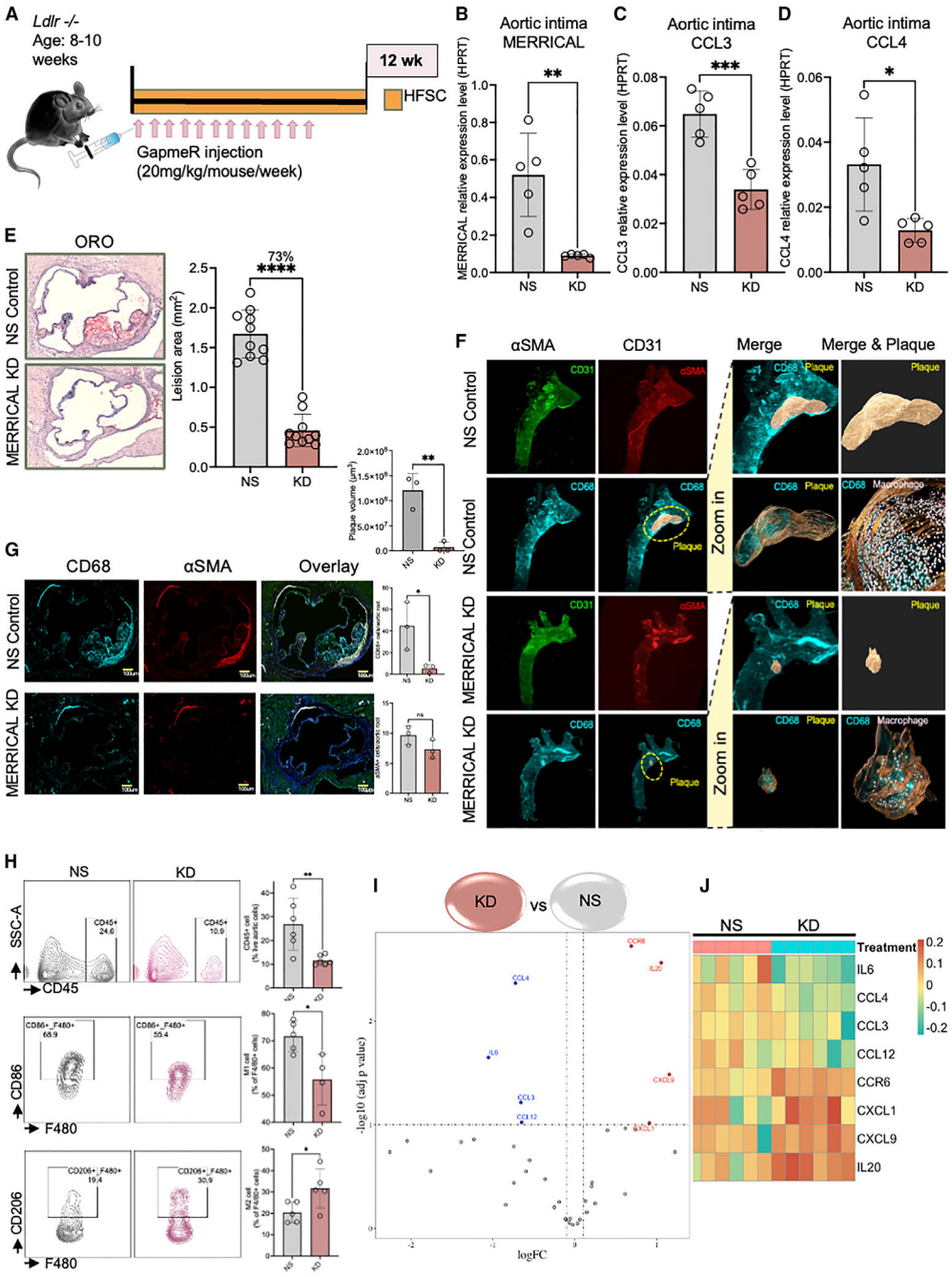

Figure 7. *MERRICAL* KD inhibits pro-inflammatory responses and atherosclerotic lesion formation *in vivo*

(A) *Ldlr*$^{-/-}$ mice on the HFSC diet were injected r.o. with NS control gapmeR or *MERRICAL* gapmeR once per week (20 mg kg^{-1} per injection per mouse) for 12 weeks.

(B–D) Quantitative real-time PCR analysis of CCL3 and CCL4 expression in the aortic intima from the NS control and *MERRICAL* KD groups (n = 5).

(E) Representative images and quantification for ORO staining in the in the aortic sinus from control and *MERRICAL* KD mice (n = 10).

Author Manuscript Author Manuscript Author Manuscript Author Manuscript

(F) Representative images and quantification of plaque volume using 3D light sheet imaging in the descending aorta from control and *MERRICAL* KD mice (n = 3). Scale bar, 500 μm.
(G) Representative image of CD68 (cyan) and α-SMA (red) staining in aortic roots and quantification of $CD68^+$ cells (n = 3). Scale bar: 100 μm.
(H) Flow cytometry analysis of aortic cells (ascending aorta to diaphragm) from control and *MERRICAL* KD mice on the HFSC diet for 12 weeks (n = 4).
(I) Volcano plot showing the mouse cytokine array in plasma from control and *MERRICAL* KD mice on the HFSC diet for 12 weeks.
(J) Heatmap showing significantly regulated cytokines in plasma from control and *MERRICAL* KD mice on the HFSC diet for 12 weeks (n = 6).
Values are mean ± SD. Significance was determined by two-tailed Student's t test for (B)–(H). *p < 0.05, **p < 0.01, ***p < 0.001, ****p < 0.0001.

Author Manuscript Author Manuscript Author Manuscript Author Manuscript

KEY RESOURCES TABLE

REAGENT or RESOURCE	SOURCE	IDENTIFIER
Antibodies		
Anti-aSMA	Sigma-Aldrich	A5228; RRID: AB_262054
Anti-CD68	Abcam	Ab201845; RRID: AB_2920880
Anti-CD31	Biolegend	102514; RRID: AB_493413
Anti-Histone H3 (tri methyl K4) antibody - ChIP Grade (ab8580)	Abcam	ab8580; RRID: AB_306649
Anti-Histone H3 (tri methyl K27) antibody [mAbcam 6002] - ChIP Grade (ab6002)	Abcam	ab6002; RRID: AB_305237
Recombinant Anti-Histone H3 (di methyl K9) antibody [Y49] - ChIP Grade (ab32521)	Abcam	ab32521; RRID: AB_732927
Histone H3K4me2 Polyclonal Antibody	Thermo Fisher	# 39141; RRID: AB_2555733
Anti-Mouse CD86	BD bioscience	563055; RRID: AB273977
Anti-mouse CD45	BD bioscience	612924; RRID: AB_2722550
Anti-Mouse CD90.2	BD bioscience	740841; RRID: AB_2740488
Anti-Actin, α-Smooth Muscle	Sigma	C6198; RRID: AB_416856
Anti-CD11b	Thermo Fisher	12-0112-82; RRID: AB_2734869
Anti-CD11c 488	Thermo Fisher	14-9761-82; RRID: AB_2572997
Anti-mouse CD206	Biolegend	141716; RRID: AB_2561991
Anti-mouse F4/80	Thermo Fisher	17-4801-82; RRID: AB_2784648
Anti-mouse CD45 BUV563	BD bioscience	612924; RRID: AB_2722550
Anti-mouse CD115 BV605	BD bioscience	743640; RRID: AB_2741650
Anti-mouse Ly6G APC	BioLegend	127614; RRID: AB_1877163
Anti-mouse Ly6C FITC	BioLegend	128006; RRID: AB_1186134
Anti-mouse CD3 Pacific blue	BioLegend	103114; RRID: AB_312978
Anti-mouse CD19 BV510	BioLegend	115545; RRID: AB2562137
Anti-mouse CD4 Pe/cy7	BioLegend	100528; RRID: 312729
Anti-histone H3 (tri methyl K4)	Abcam	Ab8580; RRID: AB_306649
Anti-histone H3 (di methyl K9)	Abcam	Ab32521: RRID: AB_372927
Anti-histone H3K4me2 Polyclonal Antibody	Thermo Fisher	39141; RRID: AB_2614985
Anti-WDR5	Cell Signaling	13105; RRID: AB_2620133
Anit-MLL1 (Kmt2a)	Active motif	61295; RRID: AB_2793585
Chemicals, peptides, and recombinant proteins		
MM102	Selleck	S7265
Lipopolysaccharides	Sigma	L2633
Mouse CCL3/MIP-1 alpha Antibody	R&D systems	AF-450-NA
Mouse CCL4/MIP-1 beta Antibody	R&D systems	AF-451-NA
DAPI	MERCK	10236276001
IMDM media	Thermo Fisher	12440053
RPMI 1640 Medium	Thermo Fisher	11875093

Author Manuscript Author Manuscript Author Manuscript Author Manuscript

REAGENT or RESOURCE	SOURCE	IDENTIFIER
Oxidized Low-density Lipoprotein (OxLDL) and DiI-OxLDL	Thermo Fisher	L34357
Triton X-100	Thermo Fisher	HFH10
DMEM	Gibco	11320–033
TRIzol reagent	Thermo Fisher	15596026
Normal Goat IgG Control	R&D systems	AB-108-C
Chromium Next GEM Single Cell 3′Reagent Kit v3.1	10x Genomics	PN-1000268
Lipofectamine™ 2000 Transfection Reagent	Thermo Fisher	11668027
EZ- Magna ChIRP RNA Interactome Kit-Isolation and characterization of non-coding RNA:chromatin complexes	Sigma	17–10495
RNAscope 2.5 HD Reagent Kit-Red	Advanced Cell Diagnostics	Customized
High-Capacity cDNA Reverse Transcription Kit	Thermo Fisher	4368814
Universal Magnetic Co-IP Kit	Active Motif	54002
SimpleChIP Enzymatic Chromatin IP Kit	Cell Signaling	9003
CUTANA™ ChIC/CUT&RUN Kit	EpiCypher	14–1408
Vybrant™ Phagocytosis Assay Kit	Thermo Fisher	V6694
Deposited data		
RNA sequencing data of NS control and MERRICAL KD BMDM	This paper	GSE235419
Experimental models: Cell lines		
bEND.3 cell	ATCC	CRL-2299
Experimental models: Organisms/strains		
C57BL/6J	Jackson	000664
Ldlr−/−	Jackson	002207
Oligonucleotides		
MERRICAL GapmeR	Qiagen	LG00788971-FZA -
Non specific control (NS) GapmeR	Qiagen	LG00000001 -FZA -
Recombinant DNA		
pcDNA3.1		N/A
pBluescript SK II+		N/A
p3xFLAG-CMV-14 expression vector		N/A
Software and algorithms		
Prism Graphpad 9	GraphPad Software	https://www.graphpad.com/features
RStudio	RStudio Team, 2020	https://cran.r-project.org/bin/macosx/
Python 3	Python	https://www.python.org/
Seurat package v4.1.1	Satijalab	http://satijalab.org/seurat/